Isotopically zoned carbonate cements in Early Paleozoic sandstones of the Illinois Basin: $\delta^{18}O$ and $\delta^{13}C$ records of burial and fluid flow

Adam C. Denny [a,*], Reinhard Kozdon [b], Kouki Kitajima [a], John W. Valley [a]

[a] Department of Geoscience, University of Wisconsin, Madison, WI 53706, USA
[b] Lamont-Doherty Earth Observatory, Columbia University, New York, NY 10964-1000, USA

ABSTRACT

SEM/SIMS imaging and analysis of $\delta^{18}O$ and $\delta^{13}C$ in sandstones from a transect through the Illinois Basin (USA) show systematic μm-scale isotopic zonation of up to 10‰ in both carbonate and quartz cements of the middle-Ordovician St. Peter and Cambrian Mt. Simon formations. Quartz $\delta^{18}O$ values are broadly consistent with the model of Hyodo et al. (2014), wherein burial and heating in the Illinois Basin is recorded in systematically zoned quartz overgrowths. Observations of zoned dolomite/ankerite cements indicate that they preserve a more extended record of temperature and fluid compositions than quartz, including early diagenesis before or during shallow burial, and late carbonates formed after quartz overgrowths. Many carbonate cements show innermost dolomite with $\delta^{18}O$ values (21–25‰ VSMOW) that are too low to have formed by deposition at low temperatures from ancient seawater ($\delta^{18}O > -3$‰) and most likely reflect mixing with meteoric water. A sharp increase in Fe content is commonly observed in zoned carbonate cements to be associated with a drop in $\delta^{18}O$ and an abrupt shift in $\delta^{13}C$ to higher or lower values. These changes are interpreted to record the passage of hot metal-rich brines through sandstone aquifers, that was associated with Mississippi-Valley Type (MVT) Pb-Zn deposits (ca. 270 Ma) of the Upper Mississippi Valley. Local variability and individual trends in $\delta^{13}C$ are likely controlled by the sources of carbon and the degree to which carbon is sourced from adjacent carbonate units or thermal maturation of organic matter. Quartz overgrowths in sandstones provide an excellent record of conditions during burial, heating, and pressure-solution, whereas carbonate cements in sandstones preserve a more-extended record including initial pre-burial conditions and punctuated fluid flow events.

© 2017 Elsevier B.V. All rights reserved.

1. Introduction

Diagenetic cements preserve a record of physical, chemical, and biologic processes during mineral growth, and control the porosity and permeability of most sedimentary rocks. They form under low temperature (<200 °C) conditions as original sediments interact and react with interstitial pore waters. Patterns of diagenetic mineral growth and dissolution, combined with chemical and isotopic zoning within a micron-scale mineral overgrowth, can preserve evidence of initial depositional conditions, burial and compaction, pressure solution, mineral alteration, hydrocarbon generation, ion fluxes, thermal events, and pulses of fluid flow—meteoric or otherwise (Longstaffe, 1989; Worden and Burley, 2003; Morad, 2009). The diagenetic development of mineral overgrowths and other cementing phases plays the dominant role in lithifying sandstones, and is often a major control on the porosity and hydraulic conductivity of sandstone aquifers and reservoirs. Improving our understanding of diagenesis and its influences on porosity remains a priority for mapping hydrocarbon and groundwater reservoirs, understanding fluid flow histories, and optimizing carbon sequestration.

Stable isotope ratios can provide sensitive records of temperature and fluid composition and are a powerful tool for interrogating questions relating to basin evolution. Diagenetic carbonate cements are typically analyzed for stable isotope ratio by conventional acid-extraction and gas-source mass spectrometry (Urey, 1948). This method requires samples, typically >50 μg, that are acquired by microdrilling, by crushing and sieving, or by differential dissolution in acid. However, these techniques homogenize discrete cementation events, they are susceptible to contamination, and they can't resolve the micron-scale isotopic zonation often present in overgrowth textures. In contrast, Secondary Ion Mass Spectrometry (SIMS) uses samples 10^4 to 10^6 times smaller and can resolve variation at the μm-scale. The in situ nature of the measurement allows correlation to imaging that documents overgrowth textures and analysis by SEM or other means (Valley and Kita, 2009; Pollington et al., 2011, 2016; Śliwiński et al. 2016c). Recent advances in the analysis of carbonate minerals by SIMS allow in situ measurements of $\delta^{18}O$ and $\delta^{13}C$ from domains 1–10 μm in diameter and ≤2 μm deep. Spot-to-spot reproducibility (external precision) of ± 0.3‰ (2SD) is attainable for $\delta^{18}O$ with a 10 μm spot; for $\delta^{13}C$ precision of ± 0.7‰ (2SD) is attainable with a 6 μm spot (Valley and Kita, 2009).

* Corresponding author.
E-mail addresses: acdenny@wisc.edu (A.C. Denny), rkozdon@ldeo.columbia.edu (R. Kozdon), saburo@geology.wisc.edu (K. Kitajima), valley@geology.wisc.edu (J.W. Valley).

With the proper use of standards, accuracy approaches precision for stoichiometric minerals like quartz (Pollington et al., 2011). Accuracy for minerals with solid solution, like dolomite, depends on the quality of standards (Śliwiński et al., 2016a,b).

In order to explore the extent to which micron-scale isotopic variation in diagenetic cements preserves a record of thermal and fluid histories, a suite of samples was collected from the lower Paleozoic St. Peter and Mt. Simon sandstones of the Illinois Basin. The development of SIMS standards for analysis of Ca-Mg-Fe carbonates significantly improves accuracy of micron-scale records of $\delta^{13}C$ and $\delta^{18}O$ fluctuation during dolomite cementation (Śliwiński et al., 2016a,b,c). The new capabilities of SIMS analysis permit a greater focus and closer interrogation of complex, previously unrecognized isotopic trends. This study integrates new imaging, elemental and stable isotope data for zoned calcite, dolomite/ankerite, and quartz cements into the history of fluid flow, mineral dissolution, alteration, and reprecipitation in the sedimentary rocks of the Illinois Basin (Clayton et al., 1966; Hoholick et al., 1984; Bethke, 1986; Pitman and Spötl, 1996; Fishman, 1997; Pitman et al., 1997; Chen et al., 2001; Kelly et al., 2007; Pollington et al., 2011, 2016; Hyodo et al., 2014; Śliwiński et al. 2016c). A total of 2176 analyses (727 dolomite/ankerite, 158 quartz, and 1291 standard analyses) are reported (Appendices A and B). In conducting this study, we sought to determine: 1) the range in isotopic variability present in zoned dolomite/ankerite cements in sandstones; 2) the relation between quartz and carbonate cements; 3) the range of diagenetic history recorded in zoned dolomite/ankerite cements; and 4) whether such isotopic histories would show regional correlations in the Illinois Basin.

1.1. Geological setting

The Illinois Basin contains a mixed sedimentary sequence, including Cambrian to Carboniferous sandstones, shales, and carbonates. It is bounded to the north by the Wisconsin Arch and Dome, to the east by the structural highs of the Cincinnati Arch, and to the southwest by the Ozark Dome. The early Paleozoic sediments contain several well-sorted quartz arenite sandstone units, which serve as important regional aquifers (Mai and Dott, 1985; Bethke, 1986; Arnold et al., 1997). Of these, the Mt. Simon Sandstone and St. Peter Sandstone are of special interest as flow conduits to ore-forming fluids of Mississippi Valley-Type deposits (Sverjensky, 1986; Bethke and Marshak, 1990; Rowan and Goldhaber, 1995; Rowan et al., 2002). More recently, the mature, early Paleozoic quartz arenites of the Upper Midwest, including the St. Peter, Mt. Simon, Jordan, and Wonewoc formations, have been mined as sources of high quality proppant sand (Benson et al., 2015). The Mt. Simon and St. Peter have also recently been explored as potential reservoirs for carbon sequestration, and the Mt. Simon is currently the target of an injection experiment managed by the Midwest Geologic Sequestration Consortium (MGSC). One million tons of carbon dioxide were injected in Decatur, IL over a three-year period between 2011 and 2014 (Berger et al., 2009; Leetaru and McBride, 2009; Bowen et al., 2011; Kheshgi et al., 2012; Leetaru and Freiburg, 2014; Śliwiński et al., 2017).

The basal Mt. Simon sandstone unconformably overlies the Precambrian bedrock throughout much of the region, and is Upper Cambrian in age (Driese et al., 1981; Lovell and Bowen, 2013). It was deposited in a primarily near-shore environment dominated first by braided rivers and later by deltaic systems as transgression occurred (Lovell and Bowen, 2013). It is broadly divided into three lithostratigraphic subunits: an upper low-permeability clay-rich unit, a middle quartz-rich unit, and a lower arkosic sandstone that in places grades into conglomerate near the unconformity with underlying Precambrian bedrock. The middle unit dominates by volume, and is considered a major aquifer/reservoir (Bowen et al., 2011). Carbonate cement distributions in the Mt. Simon were mapped by Hoholick et al. (1984), although sampling was sparse. More recently, Bowen et al. (2011) analyzed 150 thin

sections and concluded that carbonate cements are concentrated near the top of the Mt. Simon, close to the clay and carbonate-rich Eau Claire formation that conformably overlies and caps the Mt. Simon sandstone.

Outcropping in central Wisconsin, the Mt. Simon dips shallowly south towards the depocenter of the Illinois Basin near what is the present-day Illinois-Kentucky border (Fig. 1), where it reaches depths of 5 km. Studies of vitrinite reflectance from Pennsylvanian coals, apatite fission-tracks, and illite-smectite distribution in the Devonian New Albany shale have suggested that the Mt. Simon was 1–3 km deeper in southern Illinois during maximum burial than present day (Damberger, 1971; Zimmerman, 1986; Gharrabi et al., 1995). However, there is a strong possibility that these temperature-dependent depth proxies have been biased towards greater depth estimates by hot MVT fluids around 270 Ma, and modeling of this scenario would suggest closer to 1 km of eroded overburden (Rowan et al., 2002). The smaller amounts of uplift are consistent with estimates based on brittle deformation in quartz grains that suggest that the Mt. Simon in southern Illinois may have reached depths 1.5 km deeper than today during maximum burial, and that northern Illinois rocks were never buried more than a kilometer deeper than at present (Makowitz et al., 2006). Regional stratigraphy in Wisconsin preserves marine units from the Cambrian through the Devonian, but their combined thicknesses, where preserved, do not exceed 500 m. Since the Mississippian, Wisconsin has been exposed above sea level and not been capturing sediment. It can be presumed, then, that in Wisconsin 1 km of overburden serves as a conservative upper bound on paleodepth, but is perhaps an overestimate (Hoholick et al., 1984; Mai and Dott, 1985; Rowan and Goldhaber, 1996; Pitman et al., 1997).
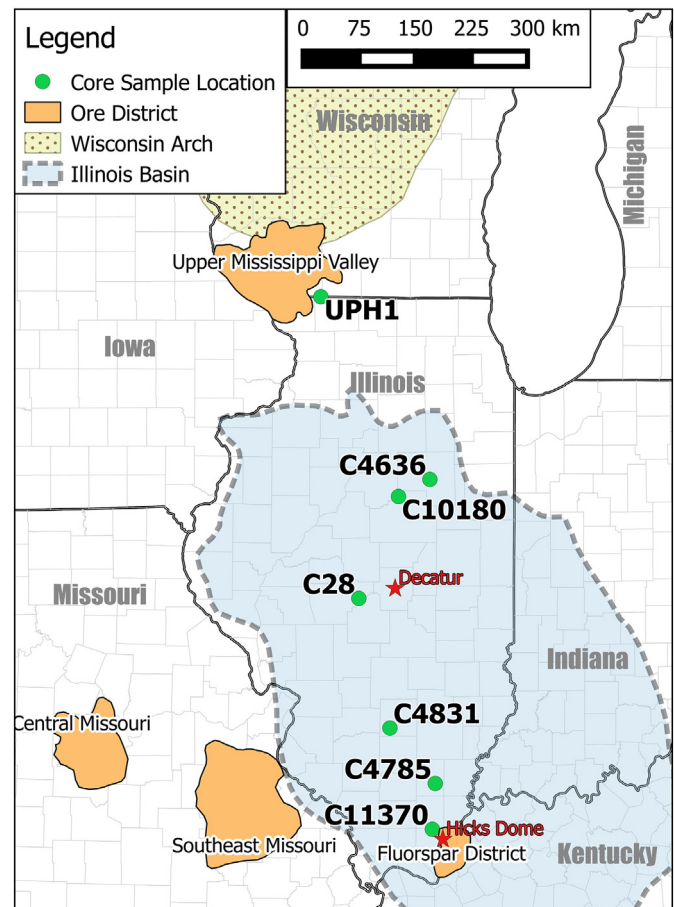

Fig. 1. Map of the Illinois Basin, with significant structures and major historically important Mississippi Valley type Pb-Zn ore districts overlain. Samples were collected from the indicated drill holes. The locations of Hicks Dome (the site of intrusive dikes in Illinois) and Decatur (the site of the MGSC CO₂ injection well) are marked with stars.

The Ordovician St. Peter sandstone is an exceptionally mature quartz arenite and represents the uppermost major aquifer/reservoir in the Illinois Basin (Mai and Dott, 1985; Arnold et al., 1997). It is divided into three lithostratigraphic subunits: The fine to medium-grained Tonti, the coarser-grained Starved Rock, and the basal Kress, which contains pebble-sized chert and dolostone associated with the underlying unconformity with the Knox Supergroup (Shaw, 1999). Once considered to be an exclusively aeolian deposit, the St. Peter is now recognized to be predominantly subtidal in origin, with the exception of portions of the Tonti subunit in Wisconsin (Dake, 1921; Mai and Dott, 1985). Attempts to map the distribution of carbonate cements within the St. Peter sandstone across Illinois do not agree well (Hoholick et al., 1984; Pitman et al., 1997); carbonate cement distributions can be strongly influenced by local porosity and mineral assemblages, and are known to be extremely patchy in drill cores (Shaw, 1991). In general, carbonate cements within the Illinois Basin tend to be of significantly higher concentration in the St. Peter than the Mt. Simon, though quartz cement still dominates (Hoholick et al., 1984; Pitman and Spötl, 1996; Pitman et al., 1997).

Previous SIMS studies on detrital quartz and quartz overgrowths in the Mt. Simon, Eau Claire (which overlies the Mt. Simon), and St. Peter formations have demonstrated that individual quartz overgrowths in the Illinois Basin show systematic zonation at the 50 to 100-μm scale with early high-δ^{18}O values (up to 32‰) in cements grading outwards to late low-δ^{18}O values (down to 17‰). Values of Δ^{18}O-(Early quartz– Late quartz) are as large as 9.1‰ within single quartz overgrowths (Pollington et al., 2011). The lowest overgrowth δ^{18}O values are typically in the outer and youngest cement. In contrast, the δ^{18}O values of detrital quartz grains average 10‰, reflecting magmatic and high-temperature metamorphic provenances. Pollington et al. (2011) proposed that quartz overgrowths derive their silica locally from pressure solution during burial, heating and compaction, and δ^{18}O trends across quartz overgrowths are indicative of their burial history. These data are best explained by a model with minimal fluid flow before the MVT event and a nearly constant δ^{18}O$_{water}$ value of −3‰ (Pollington et al., 2011; Hyodo et al., 2014). If flow was driven solely by compaction during burial and connate seawater δ^{18}O values remained unchanged, then pore waters could have been relatively constant at −3‰, which is a reasonable estimate of Cambrian-Ordovician seawater (Came et al., 2007; Jaffrés et al., 2007; Finnegan et al., 2011; Cummins et al., 2014). This model suggests that the range of observed quartz overgrowth δ^{18}O values reflects the range expected for continuous diagenetic quartz growth, from initial precipitation temperatures around 45 °C to the maximum burial temperatures expected from a 30 °C/km geotherm. The systematic δ^{18}O-zoning thus suggests that most quartz overgrowth developed prior to the fluid flow event that formed the ore deposits of the Upper Mississippi Valley.

1.2. The Upper Mississippi Valley ore-forming event

The Illinois Basin is thought to have experienced at least one major fluid flow event where mobilized warm, metal-rich brines moved up dip through its sandstone aquifers. As these fluids reached the basin margins, in places where they breached overlying aquitards, they interacted with Ordovician carbonates to precipitate the galena, sphalerite, pyrite, and fluorite mineralization of the Mississippi Valley-Type (MVT) deposits (Sverjensky, 1986). Fluids travelled over 500 km to reach southwestern Wisconsin, where the Upper Mississippi Valley (UMV) district is located (Fig. 1). Rb/Sr dates obtained from UMV sphalerite indicate an age of ~270 Ma for deposition of the MVT deposits (Brannon et al., 1992). On the basis of organic maturity in shales, Zn dispersion modeling, and thermal diffusion modeling, the duration of UMV formation, and possibly the period of fluid movement in the Illinois Basin, is estimated to have been around 200,000 years (Barnes and Lavery, 1977; Gize, 1984; Hatch et al., 1986; Rowan and Goldhaber, 1995). Fluid inclusion temperatures obtained from sphalerite in the UMV ore district generally fall between 100 and 150 °C at paleodepths of <1 km (McLimans, 1977; Arnold et al., 1997).

Numerical modeling of basin compaction and tectonics suggests that these mineral deposits were a result of the northwards gravity-driven flow of hydrothermal brines associated with the uplift of the southern margin of the basin during the Permian. Before the Permian, purely compaction-driven fluids are modeled to produce updip flow rates on the order of a few meters per thousand years, which cannot explain the high temperatures and large fluid flux observed in the UMV deposits. In contrast, flow rates on the order of several kilometers per thousand years are predicted for gravity-driven flow after uplift of the Pascola arch to the south, and modeling suggests such flow rates are sufficient to disturb the geotherm, producing temperatures up to 120 °C at shallow depths in the UMV during the 270 Ma MVT event (Bethke, 1986; Bethke and Marshak, 1990; Arnold et al., 1997). In addition, magmatic intrusion into the thickest part of the sedimentary sequence may have elevated the geotherm in the deepest part of the basin and encouraged fluid mobilization through hydrothermal circulation; modeling of a hybrid heat source such as this is consistent with preexisting data (Rowan et al., 2002). Intrusive igneous breccias associated with Hicks Dome and the Fluorospar district in southern Illinois have yielded ^{40}Ar/^{39}Ar ages of around 272 Ma, coincident with UMV ores and other dated diagenetic/thermal events throughout the region (Reynolds et al., 1997).

Numerous studies have investigated modern formation waters and porewater-rock interactions within the Illinois Basin, and though they rarely sample the deeper strata of the basin, they nonetheless might provide a basis for constraining the basin's more recent δ^{18}O$_{fluid}$ history (Clayton et al., 1966; Stueber et al., 1987, 1993; Stueber and Walter, 1991; Labotka et al., 2015). As is typical for deep sedimentary basins in other parts of the world, formation waters depart from the meteoric water line in δ^{18}O-δD space towards positive δ^{18}O values due to prolonged water-rock interaction. The first study to investigate these trends in the Illinois Basin found in situ δ^{18}O$_{porewater}$ values up to +4‰ VSMOW (Clayton et al., 1966). However, more recent study of Mt. Simon formation waters failed to find δ^{18}O$_{porewater}$ higher than −2‰, and isotopic values deviated significantly from Clayton's δ^{18}O-δD trend (Labotka et al., 2015). These differences may simply reflect modern regional isotopic variability in formation fluids. Neither study measured in situ temperatures higher than 70 °C or deeper than ~2 km, and the compositions of modern brines deeper in the basin have not been measured. Complicating matters, hydrothermal fluids would be expected to promote both water-rock interaction and advective mixing with meteoric waters, and there is no reason to expect modern isotopic fluid compositions to preserve the ore-forming fluids. Fluid inclusions from UMV minerals (sphalerite, galena, barite) possess δ^{18}O$_{inclusion}$ values in the range from −2.7 to +5.7‰, with a clustering of values between +1.5 and +5.7‰, suggesting δ^{18}O$_{water}$ compositions of MVT fluids at 270 Ma were positive (McLimans, 1977). These values for the MVT brines are interpreted to be shifted from the original deep-basin waters by interaction with high-δ^{18}O carbonates and silicates, and may provide supporting evidence for a positive ^{18}O value of MVT fluids.

2. Methods

2.1. Sample collection

Forty-two samples from seven drill cores were collected in a N-S transect roughly bisecting the state of Illinois (Figs. 1, 2). All St. Peter sandstone samples were collected from the submarine facies. Samples are from drill cores and cuttings that are curated at the Illinois State Geological Survey and the Wisconsin Geological & Natural History Survey. During sampling, carbonate-cement-rich zones identified by prior researchers were preferentially targeted (Hoholick et al., 1984; Shaw, 1991; Pitman et al., 1997), which provide samples that contained multiple diagenetic phases in close proximity. Samples from well
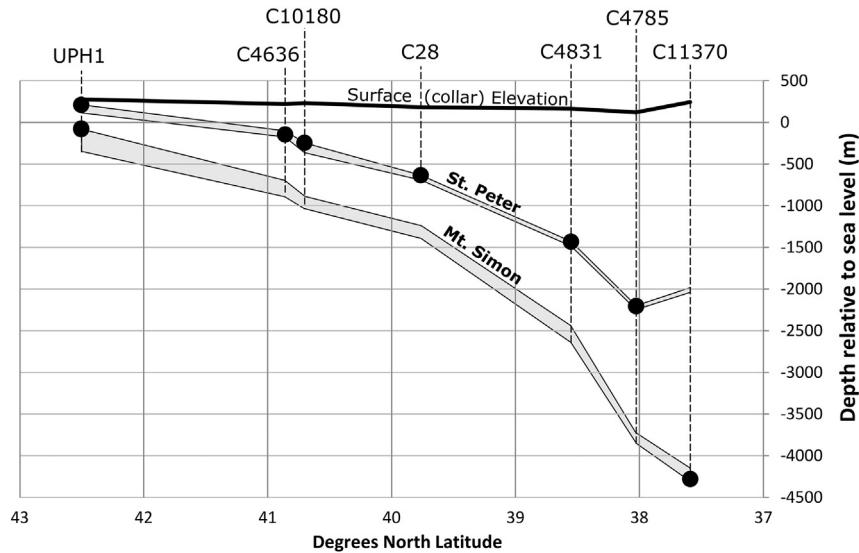
Fig. 2. N-S transect from UPH1 to C11370 (Fig. 1) displaying the depths of the Mt. Simon and St. Peter sandstones in the Illinois Basin, as well as the full depth of drill holes (vertical dashed lines) and core sample locations (black dots). Note that preserved core available for sampling often only covered a portion of the full extent of each drill hole. All depths are relative to sea level.

C11370 are drill cuttings collected at 4525 m (below collar), as no core exists from those depths. Samples of the St. Peter cover a drill hole depth range of around 70 m to 2300 m, and samples from the Mt. Simon range from 350 m to 4500 m (Table 1).

Before processing, samples were impregnated with epoxy to provide maximum preservation of friable sandstones and delicate pore-filling minerals. Carbonate cements and other diagenetic relations were then identified either through optical means (transmitted polarized light or binocular microscope) or imaging of polished surfaces with a Hitachi S3400-N scanning electron microscope (SEM) in variable pressure mode. Of the samples in which carbonates were identified, 15 were ultimately cast and polished in epoxy mounts, and 11 were analyzed by SIMS.

2.2. Sample preparation

Upon identification of zoned carbonates of interest, cubes of rock roughly 1 cm on a side were cut with a diamond saw and cast in epoxy in 2.54 cm diameter molds. In the center of each round was mounted the UWQ-1 quartz standard (Kelly et al., 2007) and the UW6220 dolomite standard (Śliwiński et al., 2016a,b). Mounts were

then ground and polished (to 0.25 μm diamond) and checked for flatness using a reflected light microscope and white light profilometer.

Prior to analysis by SIMS, chemical zoning in carbonate cements was imaged with backscattered electrons (BSE) at high vacuum by SEM. The large difference in atomic number between magnesium and iron results in greater intensity of backscattered electrons and a brighter BSE image for higher (more ankeritic) iron content (Fig. 3). Areas of particularly interesting micron-scale features were identified and imaged in detail prior to SIMS analysis, and special care was taken to preserve them during the additional cleaning and polishing required for Electron Probe Micro-Analysis (EPMA) and SIMS.

2.3. SIMS analysis of diagenetic cements

Values of $\delta^{18}O$ and $\delta^{13}C$ were obtained with a CAMECA IMS 1280 at the WiscSIMS laboratory, Dept. of Geoscience, University of Wisconsin-Madison. SIMS analysis procedures are reported in previous studies (Kita et al., 2009; Valley and Kita, 2009; Śliwiński et al., 2016a,b). Samples are exposed to a focused primary beam of $^{133}Cs^+$ ions with a 10 kV accelerating potential, which sputters sample atoms and excavates a pit in the surface (pit sizes ranged, depending on session requirements,

Table 1
Sample names, corresponding sample depths, and the locations and unique API numbers of the cores analyzed in this study. Formation tops and bases are from the Wisconsin Geological and Natural History Survey (WGNHS) and Illinois State Geological Survey (ISGS).

Sample #	Sample depth (m, rel. to sea level)	Sample depth (m, from collar)	Sample depth (ft, from collar)	Formation name	Formation top, base (m, from collar)	Latitude (decimal °)	Longitude (decimal °)	Core API
UPH1-212	211.2	64.6	212	St. Peter	63.4, 160.9	42.5056	−89.8521	121772131500
UPH1-212f	211.2	64.6	212	St. Peter	63.4, 160.9	42.5056	−89.8521	121772131500
UPH1-1144	−72.8	348.7	1144	Mt. Simon	355.1[a], 574.2	42.5056	−89.8521	121772131500
UPH1-1170	−80.8	356.6	1170	Mt. Simon	355.1, 574.2	42.5056	−89.8521	121772131500
C4636-1202	−143.9	366.4	1202	St. Peter	324, 398.4	40.86	−88.5422	121050073900
C10180-1561	−244.1	475.8	1561	St. Peter	477.6, 595.3	40.7038	−88.9191	121130053500
C28-2674.5	−633.5	815.2	2674.5	St. Peter	815.3, unknown[b]	39.7651	−89.3957	121670011500
C4831-5238.5b	−1431.8	1596.7	5238.5	St. Peter	1595.0, 1649.0	38.5522	−89.0225	121210519800
C4785-7616	−2201.6	2321.4	7616	St. Peter	2318.3, 2364.6	38.0265	−88.4778	120650345000
C4785-7623	−2203.7	2323.5	7623	St. Peter	2318.3, 2364.6	38.0265	−88.4778	120650345000
C4785-7624	−2204	2323.8	7624	St. Peter	2318.3, 2364.6	38.0265	−88.4778	120650345000
C11370-14845	−4278.2 to −4281.2	4523.2 to 4526.3	14,840 to 14,850	Mt. Simon	4501.9, unknown[c]	37.5896	−88.5128	121512030200

[a] While UPH1-1144 lies above the official contact as defined by the WGNHS, our conclusion based on the petrography is that UPH1-1144 would have been well exposed to fluids in the Mt. Simon proper for much of its history. The rock is quartz sand supported above and below the contact, and there is a steady drop in the portion of dolomite, ankerite and siderite that fills the pore space as one moves down into the Mt. Simon. The late stage siderite in UPH1-1144 is porosity filling, indicating that substantial porosity existed prior to siderite formation.

[b] Formation bottom not reached during drilling. Maximum core depth is 832.7 m.

[c] Formation bottom not reached during drilling. Maximum core depth is 4554.3 m.
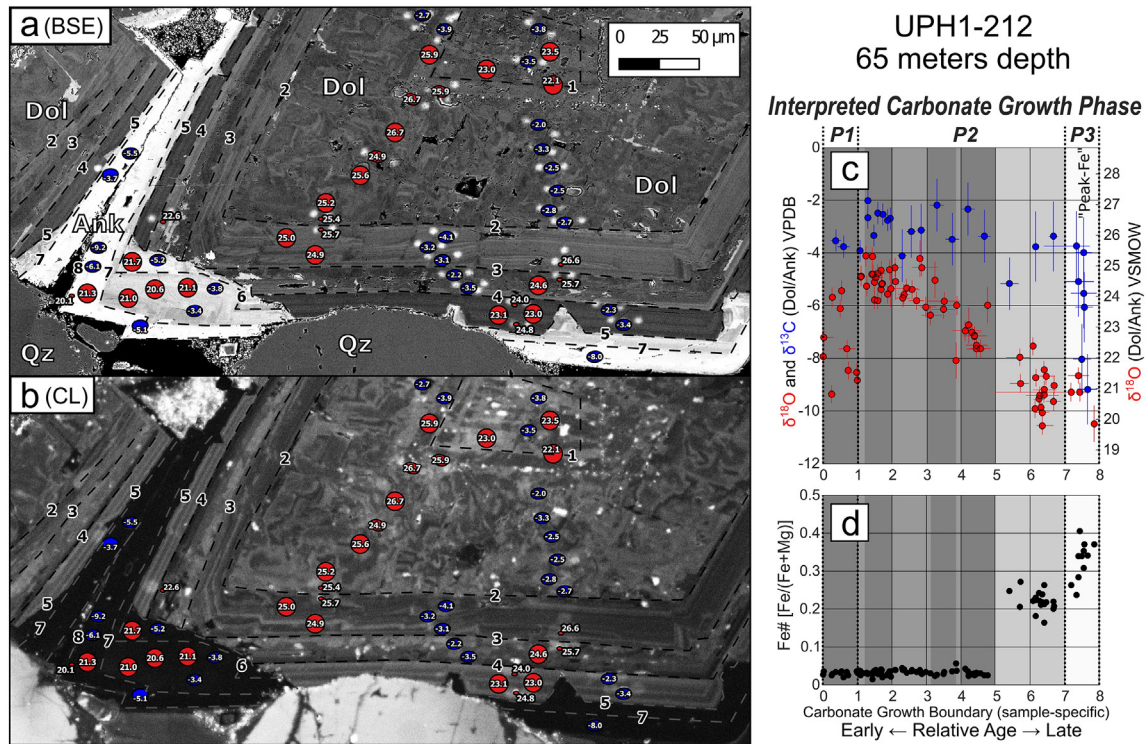
Fig. 3. (a) A representative BSE image of zoned dolomite/ankerite cement found in St. Peter sample UPH1-212, from 65 m below collar. SIMS analysis pits are drawn to scale: red ovals for $\delta^{18}O$ (values in ‰ VSMOW) and blue ovals for $\delta^{13}C$ (‰ VPDB). Dashed black lines indicate recognizable shifts in Fe content ("Growth Boundaries"), visible in BSE imaging of all carbonate cement grains analyzed, that were used to compare $\delta^{18}O$ and $\delta^{13}C$ trends across multiple grains. These growth boundaries can be correlated within a sample and are numbered 1 to N (N = 8 in Fig. 3) from the earliest cement to the latest. Oval white patches are locations analyzed by EPMA. (b) Blue-filter SEM-CL image showing the same area as in (a). (c) $\delta^{18}O$ and $\delta^{13}C$ trends from all dolomite/ankerite cements in this sample, normalized to the boundaries denoted in a and b. Grayscale shading is meant to approximate the banding present in the BSE image (a). Vertical error bars for $\delta^{18}O$ and $\delta^{13}C$ represent the 2SD precision of analysis. Horizontal error bars approximate the SIMS pit width normalized to the local width between boundaries. (d) Trends in Fe# from cement interior to rim, determined by EPMA. (For interpretation of the references to colour in this figure legend, the reader is referred to the web version of this article.)

from 12 to 3 μm in diameter, and were 2 μm deep or less). The sputtered secondary ions are accelerated into a double-focusing mass spectrometer, where ions are sorted by mass/charge and measured simultaneously with an array of Faraday cup (FC) and/or electron multiplier (EM) ion counting detectors (FC/FC for 10 μm O spots; EM/FC for C or 3 μm O spots).

The SIMS method has an instrumental bias, or instrumental mass fractionation (IMF), that results from the sputtering, transmission and detection of secondary ions. Bias varies with the composition and crystal structure of the sample and must be corrected through the careful use of standards. Commonly for solid solutions like those in the carbonate mineral family, a working curve is constructed and EPMA analyses are required for each sample analysis spot to obtain accurate major elemental compositions (Hervig et al., 1992; Eiler et al., 1997; Valley and Kita, 2009). For the dolomite/ankerite solid solution, $\delta^{18}O$ instrumental biases have been observed to vary by 10‰ or more, and $\delta^{13}C$ by up to 5‰, between magnesium and iron-rich end members, with dolomite values being especially sensitive to small changes in the amount of iron. A suite of 14 carbonate standards was developed by Śliwiński et al. (2016a,b) that tightly constrain the instrumental bias trend, which is systematic but curved and highly non-linear across the dolomite/ankerite solid solution. A linear correction between dolomitic and ankeritic end members would yield values that are incorrect by as much as 5‰ for $\delta^{18}O$ in the Fe# 0.15 to 0.3 range (Fe# = Fe/[Fe + Mg], Fe and Mg in atomic %) (Śliwiński et al., 2016a). This can be corrected with careful use of a suite of standards spanning a range of dolomite/ankerite compositions; Appendix C contains an example of such a working curve. The full suite of standards used to generate these corrections was not readily available at the beginning of this study. However, the shape of the bias vs. Fe# working curve is reproducible from session to session and this allowed a refined correction

of earlier sessions using a 3-parameter Hill-function fit (Śliwiński et al., 2016a,b). The sample analyses were bracketed by either quartz standard UWQ-1 or by dolomite standard UW6220, with analyses bracketed by a standard of the same phase whenever possible (carbonate bracketed by carbonate, quartz bracketed by quartz). Additional details of the Hill fit on a session-by-session basis as well as the standards and instrumental biases involved, are included in Appendix C.

To assist in charge compensation and prevent charging, sample mounts were coated with a layer of gold (~60 nm thick) or carbon (~25 nm thick) prior to $\delta^{18}O$ analysis, or solely with gold if $\delta^{13}C$ was to be analyzed. Sample surfaces were always repolished, washed with ethanol, rinsed repeatedly with deionized water in a sonicator, dried with a nitrogen gas stream, and inspected under a reflected light microscope to avoid contamination prior to recoating. SIMS pits were imaged post-analysis by SEM to evaluate the quality of the pits and verify that they were located in the targeted zones and phases of interest. Carbonates can be prone to fractures and contain inclusions just below the surface that are not recognizable in SEM, so verifying that there are no major pit irregularities is important in all SIMS studies (Valley and Kita, 2009). On the basis of qualitative (SEM imaging) evaluation, pits were assigned a numeric value denoting how far they deviated from an ideal appearance (3 = ideal, 0 = suspect and not used; Appendices A and B). Common observed deviations from ideal appearance include small hairline fractures intersecting the pit, or intracarbonate voids/inclusions that were exposed to the surface by the sputtering of the $^{133}Cs^+$ beam. Such small imperfections are not thought to affect SIMS carbonate isotopic values significantly. If the domain of a pit was observed to include large voids, multiple mineral phases, the suspected inclusion of epoxy in the analysis, or a rough mineral surface in the area adjacent to the pit, the analysis was considered to be potentially strongly biased and given a rating of 0. In addition to

detecting those isotopic species required to measure the isotopic ratio, simultaneous counts were made of $^{16}OH^-$ ions (for $\delta^{18}O$) or $^{13}CH^-$ ions (for $\delta^{13}C$) as a proxy for water/organic content in the analyzed volume, and to serve as a subsequent check on the reliability of the data at that location. Suspect analyses are not plotted or considered in interpretations made here; all rejected data points and reasons for rejection are provided in Appendix B.

Models for the precipitation conditions of diagenetic cements were made using the dolomite-water $\delta^{18}O$ and $\delta^{13}C$ fractionations of Horita (2014) and the low-temperature quartz-water fractionation equation of Clayton et al. (1972) as modified by Friedman and O'Neil (1977). Unless otherwise noted, all oxygen isotope ratios (carbonates, silicates, water) are reported in standard permil notation relative to one reference material (standard) for consistency, Vienna Standard Mean Ocean Water (VSMOW). For convenience, in Appendix A values of $\delta^{18}O$ are also reported relative to the VPDB scale using the conversion of Coplen et al. (1983). Carbon isotopes are reported relative to VPDB.

2.4. Electron probe micro-analysis

After SIMS analyses were made and raw values had been obtained for isotope ratios, chemical compositions adjacent to each analysis spot in carbonate were determined by Electron Probe Micro-Analysis (EPMA). Because of the sensitivity of the instrumental bias correction to Fe content, and because of the small-scale Fe-Mg zonation present in most analysis areas, it was essential that the major and minor element chemistry of the carbonate analyzed in each pit be determined. Sample mounts were carbon coated and analyzed on the CAMECA SX-51 at the Cameron Electron Microprobe Lab, Department of Geoscience, UW-Madison. Generally, two or three EPMA analyses were made per SIMS pit, with a 15 keV electron beam defocused to 2 or 5 μm at 10 or 20 nA, respectively (smaller beam sizes allowed for smaller-scale measurement of complex carbonate zonation, but a corresponding decrease in current was required to minimize damage to carbonate phases during analysis). Because EPMA accuracy is dependent on the presence of a flat sample surface, analyses were made immediately adjacent to SIMS pits as close as possible to the zone of interest based on BSE images, while still maintaining a distance of ~5 μm from pits to minimize topographic effects relative to 1–2 μm deep pits. Two to three measurements were made around each pit and care was taken to image all analysis regions post-EPMA to verify that EPMA spots recorded the chemistry of carbonates that are composition-equivalent to the SIMS pits (e.g., Fig. 3a).

3. Results

All samples are labeled (e.g., UPH1-212) using the convention: 'Drill Core ID - Depth in Feet Below Drill Collar' (Table 1); multiple mounts from the same core sample were distinguished with letter suffixes (e.g., UPH1-212f). Images showing analysis spots and isotope ratios of most regions analyzed by SIMS in this study are available in Appendix D. These images compliment the petrographic summaries.

All observed carbonates that lie in the dolomite-ankerite compositional range possess some degree of concentric banding in Fe content. These bands are interpreted to have developed during the outward growth of the carbonate cements in response to changes in local fluid and temperature conditions. In many samples, multiple zoned dolomite/ankerite grains were analyzed by SIMS to improve the resolution of isotopic trends. If the Fe variability in an individual sample's carbonate cements was systematic and easily identifiable from grain to grain, data were compiled in order of precipitation and normalized through the use of correlatable, sample-specific "Growth Boundaries" where recognizable shifts in dolomite/ankerite Fe content occur (e.g., Fig. 3). The purpose of this correlation was to test the consistency of the data from grain to grain within individual samples and to better elucidate isotopic trends recorded during carbonate growth. These

growth boundaries are thought to represent bands of time-equivalent growth in all of a sample's diagenetic cements, but these boundaries are not used for correlation from rock to rock despite similarities that exist between observed trends in all basin cements. The possibility of correlation does exist on the basis of four "Growth Phases" (see Discussion section). For the purposes of descriptive clarity, specific dolomite/ankerite growth bands will from this point on be referred to on the basis of chemistry as dolomite (Fe/(Fe + Mg) < 0.1), ferroan dolomite (0.1 < Fe/(Fe + Mg) < 0.2), or ankerite (Fe/(Fe + Mg) > 0.2) atomic ratios, after Chang et al. (1996).

3.1. Sample petrography and geochemistry

3.1.1. UPH1-212

Sample UPH1-212 was taken from near the top of the St. Peter sandstone at a modern depth of 65 m (212 ft) below the surface (Table 1). The extent of quartz cementation within this sample varies significantly across the 1-cm analysis region. Some regions contain only sparse, small (<30 μm) euhedral overgrowths, and in others, secondary quartz entirely occludes the pore space. Quartz overgrowth $\delta^{18}O$ values cluster tightly in the 26 to 28‰ range, and do not show a consistent trend towards higher or lower values between early and late overgrowths. These results are similar to those of Kelly et al. (2007), who analyzed quartz overgrowths that are interpreted to be early and low temperature from outcrops of St. Peter sandstone in southern Wisconsin.

Zoned dolomite/ankerite cements possess early-formed dolomite centers that are relatively low in $\delta^{18}O$ (22 to 24‰ VSMOW, −9 to −7‰ VPDB) (Fig. 3) (between boundaries 0 and 1), which are surrounded by higher values in the 25 to 27‰ range. These $\delta^{18}O$ values then steadily decrease to 20–22‰ for the latest cements between boundaries 7 and 8, with an intermediate region of minor but complex Fe zonation in dolomite suggestive of recrystallization (between boundaries 1 and 2), followed by a dissolution boundary (boundary 5), a thin band of ferroan dolomite (boundaries 5–6), and finally by an ankerite rim (boundaries 5–8). Values of $\delta^{13}C$, in contrast, remain consistently in the −2 to −4‰ range until after the dissolution boundary (boundary 5), at which point they trend to a more negative value of −9‰. On the basis of petrographic growth relations observed between diagenetic quartz and carbonate (Appendix E), the main quartz growth phase is thought to have occurred coincident with dolomite growth but prior to the later dissolution event and ankeritic rim.

3.1.2. UPH1-212f

Sandstone UPH1-212f was taken from the same piece of drill core as UPH1-212. Though only collected about 5 cm apart vertically (UPH1-212f is deeper), this sample is distinguished from UPH1-212 by widespread pyrite and glauconite sharing pore space with dolomites and quartz overgrowths. The main feature of interest in the sample is a fracture, approximately 1 cm long and 40 μm across, that cuts detrital quartz grains and quartz overgrowths alike (Appendix E). Layers of diagenetic quartz fill both the original porosity and line the interior of the fracture, showing that diagenetic quartz formed both prior to and after fracture formation. During analysis, attempts were made to analyze the earliest and latest overgrowths of quartz using a small (3 μm) spot. Overgrowths in this sample have a greater observed spread in quartz $\delta^{18}O$ values (26.8 to 31.9‰, small spot) when compared to UPH1-212 (26.4 to 28.2‰, mostly large spot), likely due to the smaller size of the analysis pits. Dolomite/ankerite $\delta^{18}O$ and Fe# trends are broadly similar to those seen in UPH1-212.

3.1.3. UPH1-1144

Sandstone UPH1-1144 was collected at a modern depth of 349 m below the surface, at the boundary between the Mt. Simon and the overlying Eau Claire formations, and is predominantly quartz grain supported despite its porosity being almost entirely filled with carbonates

(Fig. 4a). Dolomite/ankerite $\delta^{18}O$ values are variable between 18.9 and 25.7‰, with $\delta^{13}C$ in the − 0.6 to − 6.0‰ range. Dolomites are complexly zoned and growth was interrupted by at least two periods of dissolution. Dolomite growth appears to have terminated prior to the growth of the majority of the diagenetic quartz, as diagenetic quartz extends out from detrital grains and around euhedral dolomite rhombs (Fig. 4a). Quartz overgrowth $\delta^{18}O$ values range from 23.9 to 27.9‰. After the termination of quartz growth, carbonate growth continued with an ankeritic phase ($\delta^{18}O$ range 19.5 to 25.4‰ VSMOW, $\delta^{13}C$ down to − 13.4‰ VPDB). Due to its higher Fe-content, siderite occurs as a bright white phase in BSE imagery and clearly postdates ankerite growth.

3.1.4. UPH1-1170

Sandstone UPH1-1170 was collected from the top of the Mt. Simon, at a modern depth of 357 m below the surface. Quartz overgrowths are sparse, predate ankerite, and $\delta^{18}O$ (Qz) values fall into the 25.0 to 26.8‰ range. Dolomite was not observed, despite the close proximity

to UPH1-1144. Both ankerite and siderite are present, but are not in contact with each other. Ankerite is presumed to predate siderite based on relations in UPH1-1144, but the lack of contacts demonstrates that the later siderite did not nucleate on ankerite. Ankerite $\delta^{18}O$ values are nearly constant (16.2 to 17.8‰), while $\delta^{13}C$ values shift downwards by 6‰ from center to rim (− 7.5 to − 13.5‰).

3.1.5. C4636-1202

Sandstone C4636-1202 is a portion of a dolomite concretion from the St. Peter, roughly 2 cm in diameter, collected from drill core at a modern depth of 366 m below the surface. Analyses were concentrated near the edge of this concretion (Fig. 4b), where the highest iron contents and the largest observed swings in isotopic values were located. Pyrite is visible in hand sample and is associated with the edges of some of these concretions. Beyond the concretions, sand is extremely friable and little of the surrounding rock at this depth remained coherently preserved. Despite the size of the concretion analyzed, no appreciable shift in $\delta^{18}O$ was observed until the last 100 μm of growth,
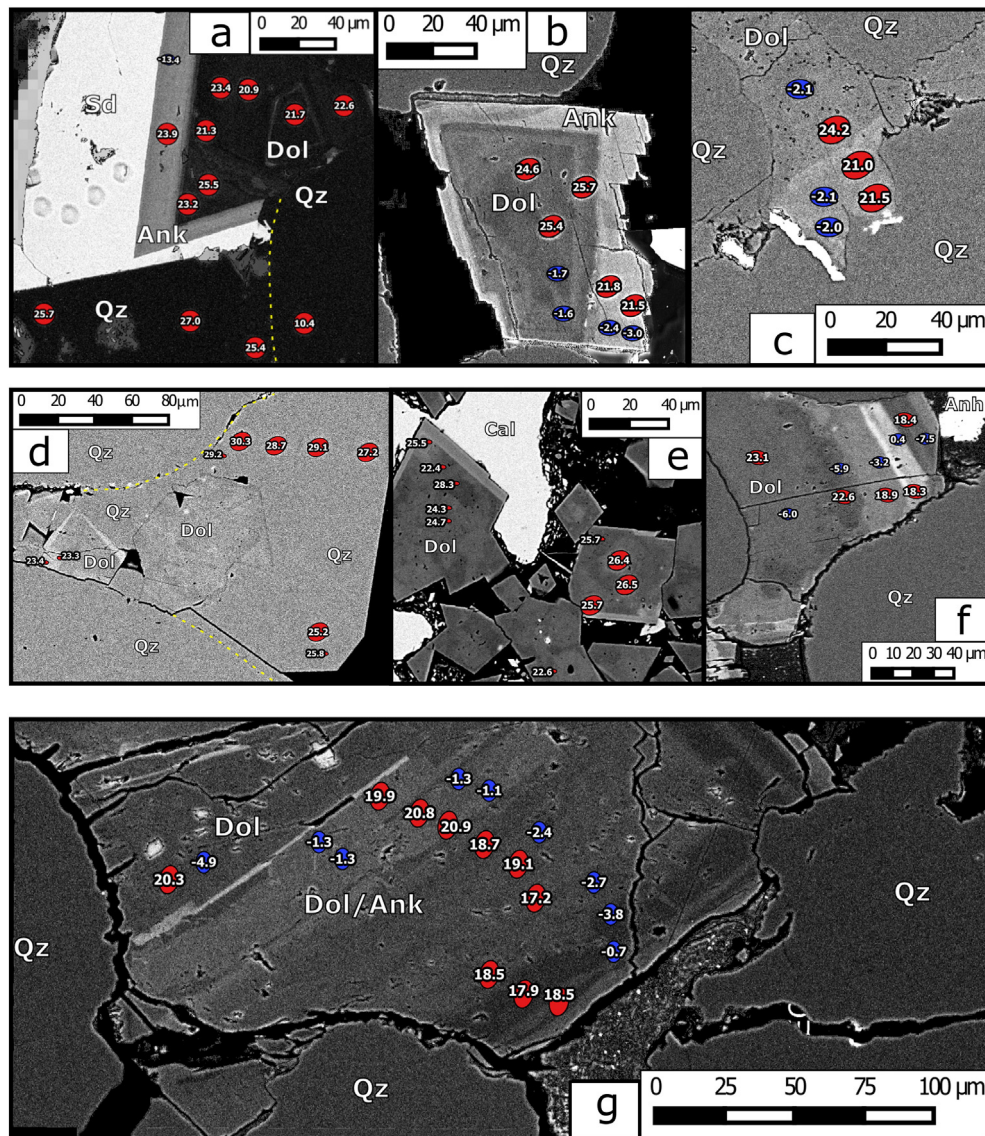
Fig. 4. SEM-BSE images providing examples of zoned dolomite/ankerite cement zonation in samples: (a) Sample UPH1–1144, Mt. Simon. (b) Sample C4636-1202, St. Peter; image shows a small rhomb at the edge of the concretion. (c) Sample C4636-1202, St. Peter; image taken in interior portion of carbonate concretion. (d, e) Sample C28-2674.5, St. Peter. (f) Sample C4785-7616, St. Peter. (g) Sample C4785-7623, St. Peter, from the rim of a carbonate concretion that extends upwards out of the field of view. Pits from oxygen isotope analysis are denoted with red ovals ($\delta^{18}O$ in ‰ VSMOW). Pits from carbon isotope analysis are blue ovals ($\delta^{13}C$ in ‰ VPDB). Yellow dashed lines demark the boundary between detrital and overgrowth quartz. Qz = Quartz, Dol = Dolomite, Ank = Ankerite, Cal = Calcite, Anh = Anhydrite. (For interpretation of the references to colour in this figure legend, the reader is referred to the web version of this article.)

where carbonate $\delta^{18}O$ values drop from 25‰ to around 21‰, coincident with an increase in Fe content. In multiple locations within this concretion, dolomite was observed to have replaced detrital quartz (e.g., Fig. 4c). Little change in $\delta^{13}C$ occurred throughout the growth history. No quartz overgrowths were observed.
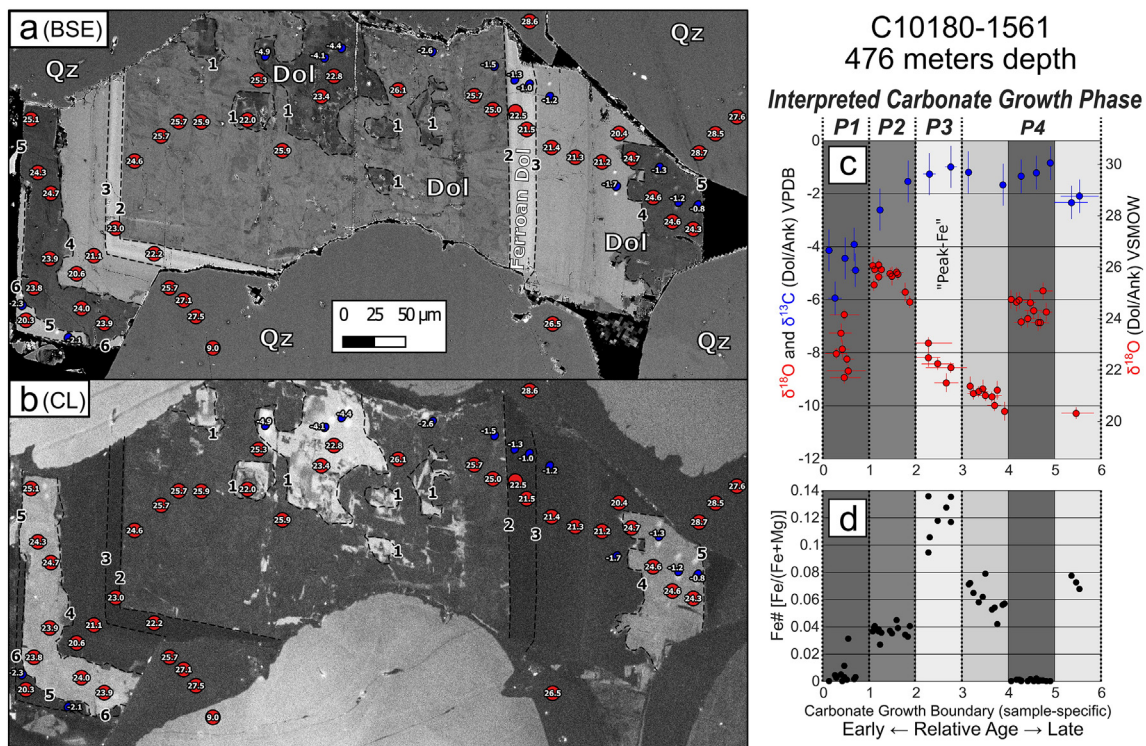
3.1.6. C10180-1561

Sandstone C10180-1561 is from the St. Peter, at a modern depth of 476 m below the surface. Dolomite/ankerite cements in this sample show a complex but consistent growth pattern from grain to grain (Fig. 5). Early innermost dolomite is low in $\delta^{18}O$ (21.7 to 24.2‰) relative to values in surrounding carbonate (between boundaries 1 and 2), and the dark irregular and patchy shapes of these central regions in BSE provide evidence that they were partially dissolved and/or recrystallized at some point in their history (Fig. 5a) (between boundaries 0 and 1). Dolomite growth subsequent to this dissolution event begins with high $\delta^{18}O$ values (26‰) and drops steadily through a band of ferroan dolomite to below 21‰, while over the same interval, $\delta^{13}C$ values rapidly rise from the -6 to -4‰ in innermost dolomite cements to the -2 to -1‰ range and hold relatively steady at -1‰ for the remainder of carbonate precipitation (Fig. 5c). The majority of quartz overgrowths ($\delta^{18}O = 25.4$ to 30.2‰) clearly postdate earlier dolomites, but likely precipitated prior to and coincident with the most Fe-rich ankeritic band (boundaries 2 to 3), based on interfingering petrographic relations between quartz and carbonate (Appendix E, k–m). Another dissolution event (boundary 4) marks the end of the decline in $\delta^{18}O$ values, and is followed by higher $\delta^{18}O$ dolomite (23.8 to 25.1‰). One final dissolution event (boundary 5) corroded this dolomite, which was followed by a final phase of carbonate growth and a return to higher Fe and lower $\delta^{18}O$ values.
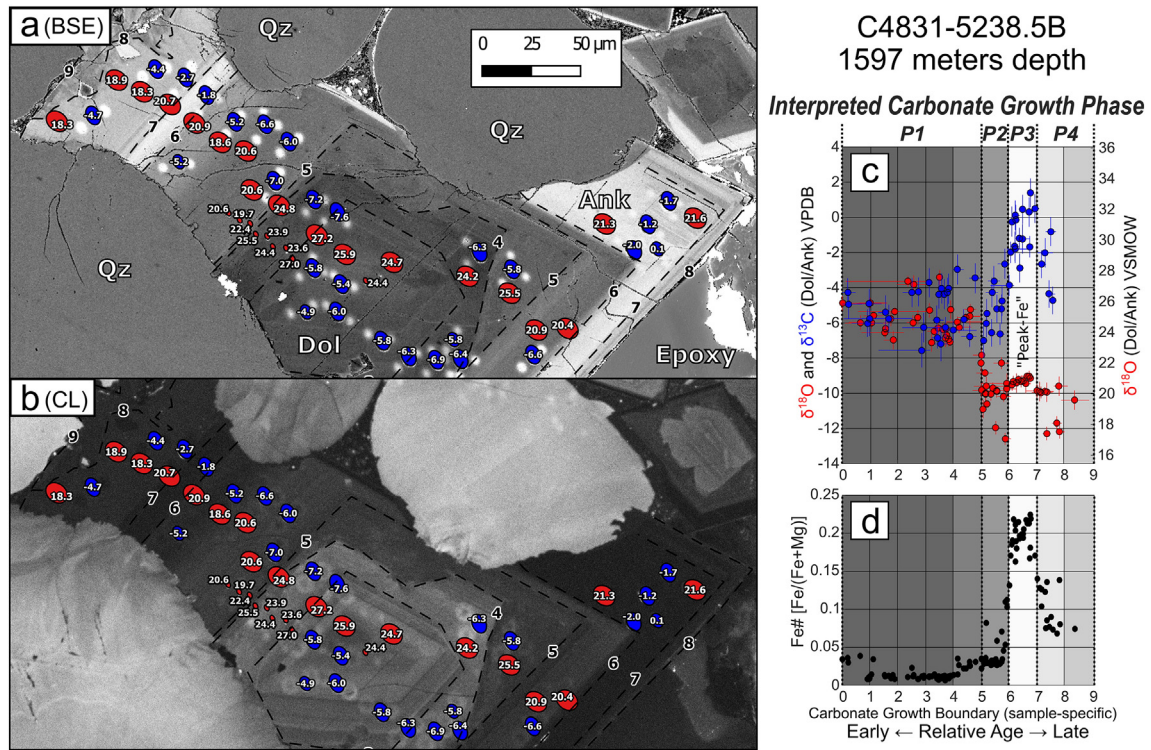
3.1.7. C28-2674.5

Sandstone C28-2674.5B is from the St. Peter, at a modern depth of 815 m below the surface (Fig. 4d,e). Dolomite cements ($\delta^{18}O$ of 22.4 to 28.3‰, $\delta^{13}C$ of -6.7 to -6.0‰) are widespread and small (<50 μm from grain center to rim) relative to those observed in other samples. Based on petrographic relations, quartz overgrowths ($\delta^{18}O$ of 25.2 to 30.3‰) postdate the majority of the dolomite precipitation, but predate a thin band of more Fe-rich dolomite that coats many of the rhombs. Carbonate precipitation ended with the growth of large calcites, >400 μm across, in portions of the sample ($\delta^{18}O$ of 19.2 to 20‰, $\delta^{13}C$ of -4 to 0‰).

3.1.8. C4831-5238.5B

Sandstone C4831-5238.5B is from the top of the St. Peter, at a modern depth of 1597 m below the surface, and just one centimeter below the base of the overlying Platteville Limestone. The lithologic transition between these two formations is quite abrupt, and focused at a thin, shaley stylolite-like dissolution boundary consuming both carbonate and quartz. The sample contains sparse quartz overgrowths ($\delta^{18}O$ of 22.3 to 25.5‰) and abundant zoned dolomite/ankerite. Innermost dolomite cement interiors are complexly zoned and experienced at least one dissolution event. From an early range of 24 to 27‰, $\delta^{18}O$ values drop sharply just prior to peak Fe content (ankerite band) and remain around 20 to 22‰ for the remainder of carbonate growth, which includes a final ferroan dolomite rim. Values of $\delta^{13}C$ in early cements are -3 to -7‰ and rise sharply with the onset of the ankerite growth phase to 0‰ (Fig. 6). Unlike many of the other samples analyzed, the sparse unetched quartz overgrowths appear to postdate ankerite growth (Appendix D), suggesting that the majority of quartz growth in this sample was unusually late, or ankerite was unusually early, possibly related to the close proximity of the sample to the overlying Platteville.

Fig. 5. (a) A representative SEM-BSE image of zoned dolomite/ankerite cement in St. Peter sample C10180-1561 from 476 m below collar. SIMS analysis pits are drawn to scale: red ovals for $\delta^{18}O$ (values in ‰ VSMOW) and blue ovals for $\delta^{13}C$ (‰ VPDB). Dashed black lines indicate recognizable shifts in Fe content ("Growth Boundaries"), visible in BSE imaging of all carbonate cement grains analyzed, that were used to compare $\delta^{18}O$ and $\delta^{13}C$ trends across multiple grains. These growth boundaries can be correlated within a sample and are numbered 1 to N ($N = 6$ in Fig. 5) from the earliest cement to the latest. Oval white patches are locations analyzed by EPMA. (b) Blue-filter SEM-CL image showing the same area as in (a). (c) $\delta^{18}O$ and $\delta^{13}C$ trends from all dolomite/ankerite cements in this sample, normalized to the boundaries denoted in a and b. Grayscale shading is meant to approximate the banding present in the BSE image (a). Vertical error bars for $\delta^{18}O$ and $\delta^{13}C$ represent the 2SD precision of analysis. Horizontal error bars approximate the SIMS pit width normalized to the local width between boundaries. (d) Trends in Fe# from cement interior to rim, determined by EPMA. (For interpretation of the references to colour in this figure legend, the reader is referred to the web version of this article.)

Fig. 6. (a) A representative SEM-BSE image of zoned dolomite/ankerite cement found in St. Peter sample C4831–5238.5B, from 1597 m below collar. SIMS analysis pits are drawn to scale: red ovals for δ^{18}O (values in ‰ VSMOW) and blue ovals for δ^{13}C (‰ VPDB). Dashed black lines indicate recognizable shifts in Fe content ("Growth Boundaries"), visible in BSE imaging of all carbonate cement grains analyzed, that were used to compare δ^{18}O and δ^{13}C trends across multiple grains. These growth boundaries can be correlated within a sample and are numbered 1 to N ($N = 9$ in Fig. 6) from the earliest cement to the latest. Oval white patches are locations analyzed by EPMA. (b) Blue-filter SEM-CL image showing the same area as in (a). (c) δ^{18}O and δ^{13}C trends from all dolomite/ankerite cements in this sample, normalized to the boundaries denoted in a and b. Grayscale shading is meant to approximate the banding present in the BSE image (a). Vertical error bars for δ^{18}O and δ^{13}C represent the 2SD precision of analysis. Horizontal error bars approximate the SIMS pit width normalized to the local width between boundaries. (d) Trends in Fe# from cement interior to rim, determined by EPMA. (For interpretation of the references to colour in this figure legend, the reader is referred to the web version of this article.)

3.1.9. C4785-7616, 7623, 7624

Sandstones C4785-7616, -7623, and -7624 are from the same core in the St. Peter (2321 to 2324 m below the surface). Zoned dolomite/ankerite cements are widespread in both 7616 and 7624, in some regions appearing to entirely fill porosity (Figs. 4f, 7), while in 7623 carbonate cements are limited to sparse concretions approximately 1 mm across (Appendix D; zonation is found at the edges of concretions, as in Fig. 4g). An interior to rim compilation of δ^{18}O and δ^{13}C data in carbonates from 7624 is provided in Fig. 7c. Isotopic trends in the carbonates of all three samples are surprisingly consistent. Initial dolomite δ^{18}O values start around 24‰, before dropping sharply at a dissolution boundary to values as low as 15‰. They rise to ~21‰ at a thin, Fe-rich band that marks the most ankeritic growth stage (boundary 4). Values of δ^{18}O then descend steadily through younger dolomite growth bands to ~17‰, before gradually climbing back up to ~20‰ at the end of carbonate precipitation. Values for δ^{13}C start around −4‰ for early growth, before rising to above 0‰ at the thin ankerite band (boundary 4). After this brief excursion, δ^{13}C values return to −4‰ and gradually rise to 0‰, drop to −5‰, and then rise again until growth ends around −3‰. Quartz overgrowths were virtually absent from 7616 and 7623, but they are abundant in regions of 7624 where zoned dolomite/ankerite was generally sparse, and appear to have mostly developed prior to the most Fe-rich ankerite growth bands. Values of δ^{18}O for diagenetic quartz range from 18.9 to 30.8‰. Sample C4785–7616 also contains anhydrite, a late phase that appears to completely postdate carbonate precipitation.

3.1.10. C11370-14845

Unlike the other samples, which were collected directly from the core, sample C11370-14845 consists of five pieces of drill cuttings <0.5 cm in size collected between 4523 and 4526 m below the surface, depths consistent with the Mt. Simon or Mt. Simon equivalent rocks. Minimal porosity remains in all five cuttings. Two of the cuttings contain a complex assemblage of glauconite, quartz, feldspar, calcite, and ankerite, with very Fe-rich rims growing at the expense of glauconite. Quartz grains show rounded detrital cores and overgrowths by CL. The glauconite and feldspar appear to be at least partially detrital in origin. Ankerite, feldspar and quartz cements came later during diagenesis. Zoned ankerites in the pair of cuttings show drops during growth from ~20 to ~14‰ for δ^{18}O and 1 to −2‰ for δ^{13}C.

The three remaining cuttings appear to have been originally feldspathic arenites with porosity filled predominantly by quartz overgrowths. K-feldspars have been partially albitized or replaced by siderite, and secondary albite is present along some detrital quartz-quartz overgrowth contacts as well. Ankerites have filled porosity in a few patchy locations. The ankerites surround rounded detrital quartz grains and at least partially predate the quartz overgrowths. Determining relative timing of the ankerites is difficult as some of the replacive carbonates have developed euhedral habits, and in places carbonates are observed to replace quartz. Ankerites fall into the 18 to 19‰ range for δ^{18}O and the −10 to −7‰ range for δ^{13}C.

It is worth noting that drill core C11370 is located within 20 km of surface-exposed dikes associated with Hick's Dome (272 Ma), and as a result may have experienced alteration by hydrothermal fluids of magmatic origin (Reynolds et al., 1997).

3.2. Overall trends

Calcite is rare and was only identified in two samples, C28-2674.5 and C11370-14845. Despite being imaged with BSE, CL, and compositionally
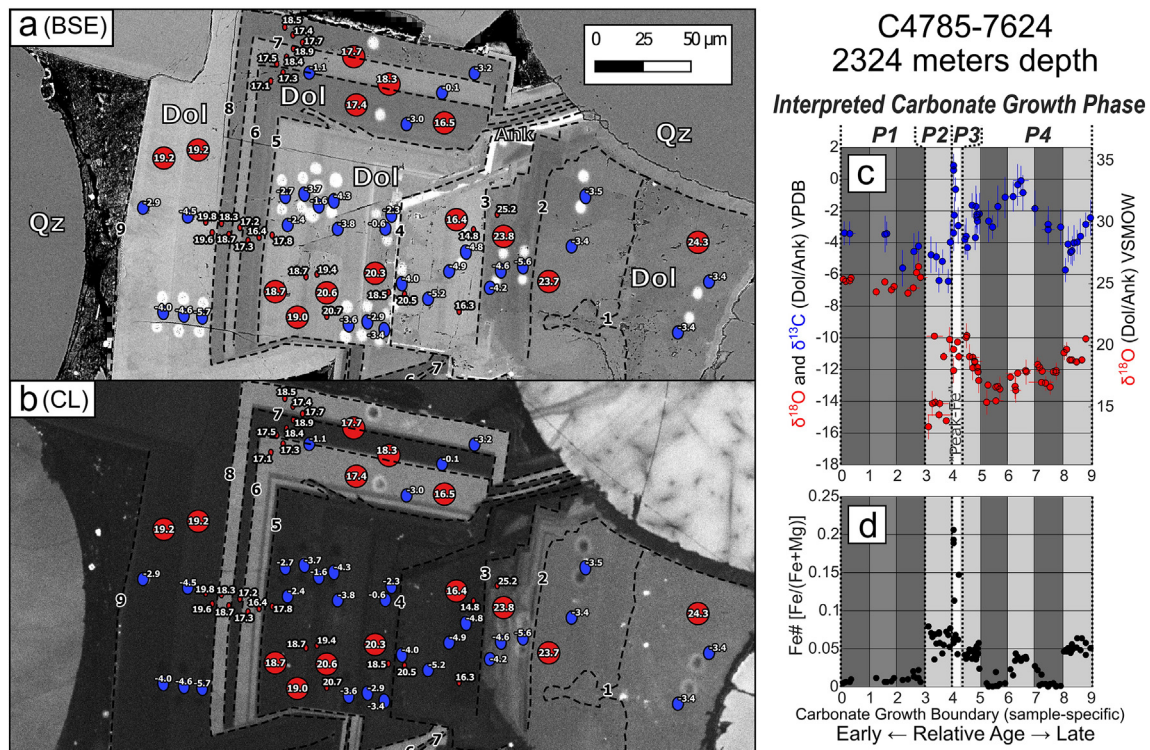
Fig. 7. (a) A representative SEM-BSE image of zoned dolomite/ankerite cement found in St. Peter sample C4785-7624, from 2324 m below collar. SIMS analysis pits are drawn to scale: red ovals for $\delta^{18}O$ (values in ‰ VSMOW) and blue ovals for $\delta^{13}C$ (‰ VPDB). Dashed black lines indicate recognizable shifts in Fe content ("Growth Boundaries"), visible in BSE imaging of all carbonate cement grains analyzed, that were used to compare $\delta^{18}O$ and $\delta^{13}C$ trends across multiple grains. These growth boundaries can be correlated within a sample and are numbered 1 to N (N = 9 in Fig. 7) from the earliest cement to the latest. Oval white patches are locations analyzed by EPMA. (b) Blue-filter SEM-CL image showing the same area as in (a). (c) $\delta^{18}O$ and $\delta^{13}C$ trends from all dolomite/ankerite cements in this sample, normalized to the boundaries denoted in a and b. Grayscale shading is meant to approximate the banding present in the BSE image (a). Vertical error bars for $\delta^{18}O$ and $\delta^{13}C$ represent the 2SD precision of analysis. Horizontal error bars approximate the SIMS pit width normalized to the local width between boundaries. (d) Trends in Fe# from cement interior to rim, determined by EPMA. (For interpretation of the references to colour in this figure legend, the reader is referred to the web version of this article.)

analyzed by EPMA, no definitive evidence of zonation in calcite was found. In C28, calcite postdates all other cements and has $\delta^{18}O$ values clustered in the 19 to 20‰ range, and $\delta^{13}C$ is mainly in the −2 to −3‰ range. In C11370, calcite is interpreted to be early, predating much of the dolomite/ankerite growth and a single analysis gave a $\delta^{18}O$ value of 24.6 and $\delta^{13}C$ of −4.6‰.

Siderite is present in Mt. Simon samples UPH1-1144, UPH1-1170, and C11370-14845 (none was observed in the St. Peter sandstone). Siderites generally have a few wt% Mg and Ca, and C11370 has minor quantities of Mn. SIMS analyses of these siderites were attempted, but a full bias correction for these phases is still being developed it is not presently possible to accurately correct the raw data to the VSMOW or VPDB scales. These data do not influence the conclusions below, and will not be discussed further.

Looking at the basin as a whole, syntaxial quartz overgrowths on detrital grains are present in nearly all samples, and show euhedral growth wherever pore space was available around detrital grains. Fibrous or opaline silica was not observed in samples for which thin sections were made, and $^{16}OH^-$ ion counts for all quartz analyses were lower than would be expected for opaline silica (Oster et al., 2017). The degree to which quartz overgrowths are present, however, is highly variable. All samples show evidence of detrital quartz dissolution at grain boundaries and/or etching of quartz in pore space, which would have released silica into pore fluids.

On the basis of observed growth relations with dolomite/ankerite, a large portion of quartz growth in the analyzed samples is thought to have occurred between two separate periods during which dolomite/ankerite growth was dominant (Appendix E). This observation is consistent with previous diagenetic studies focused on the petrography of the St. Peter cements (Pitman and Spötl, 1996; Dwyer, 2011). Detrital

quartz grains cluster around 10.2‰ (± 2.6‰ 2SD) for $\delta^{18}O$, which is consistent with previous studies (Pollington et al., 2011; Hyodo et al., 2014) and results from a high temperature igneous or metamorphic origin prior to being eroded from Precambrian bedrock (Johnson and Winter, 1999). The spread of $\delta^{18}O$ values is much wider for quartz overgrowths, that vary from 18 to 32‰ (Fig. 8), than for detrital quartz.

The zoning patterns observed in analyzed dolomite/ankerite samples share significant similarities despite differences in lithology and covering a wide geographic area. Dolomites are moderately Ca-rich, generally plotting in the 50–55% Ca range, though some ankerites show even greater enrichment in Ca (Fig. 9). All of the analyzed dolomite/ankerite cements trend towards more Fe-rich compositions near their rims, and most samples show a coincident lowering in $\delta^{18}O$ values for more Fe-rich (generally younger) cements (e.g. Fig. 7, Fig. 10a). In the three deepest drill cores studied (C4831, C4785, and C11370), these shifts in Fe content and $\delta^{18}O$ are particularly abrupt and pronounced, and are closely related to abrupt changes in $\delta^{13}C$.

Taken as a whole, $\delta^{13}C$ values appear to show two different trends with relation to Fe content. There is a positive correlation between $\delta^{13}C$ and Fe# for low Fe# carbonates, and others show a negative correlation for high Fe# carbonates (Appendix F). Generally, the correlation in St. Peter samples is positive, and the correlation in the Mt. Simon is more negative, likely due to the influence that migrating fluids on both Fe# and $\delta^{13}C$ values (discussed further in Section 4.4, below).

4. Discussion

Our new in situ data show that diagenetic carbonates record and preserve large ranges and systematic trends in stable isotope ratios during their growth history (variability up to 10‰ for $\delta^{18}O$ and up to
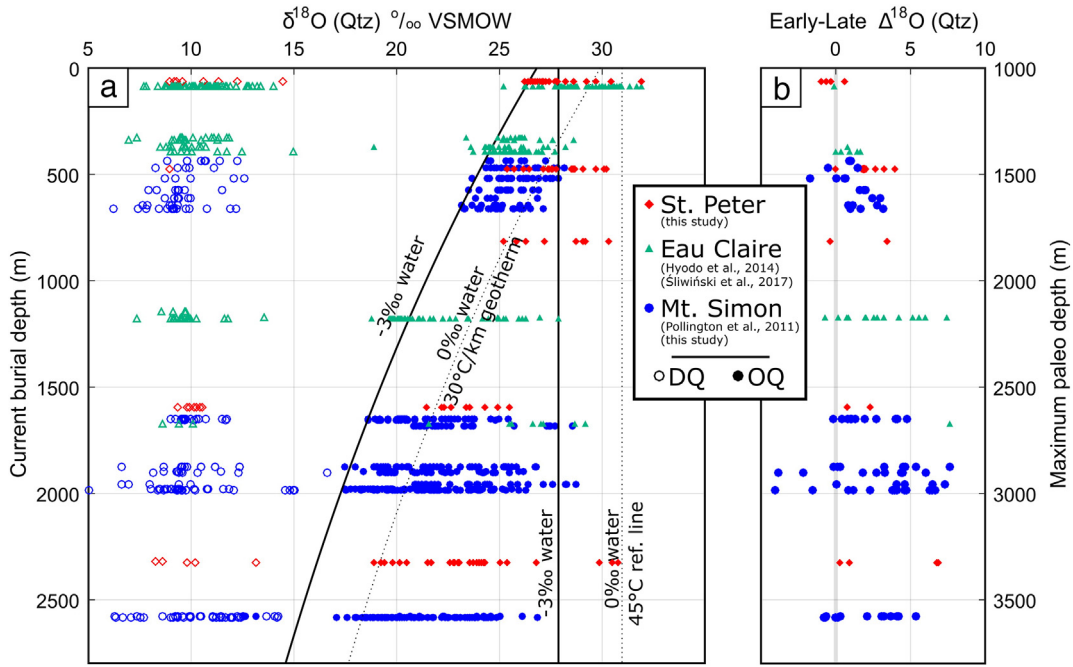
Fig. 8. (a) Plot of all SIMS quartz $\delta^{18}O$ data vs. present depth collected during the study of diagenetic quartz overgrowths in the Illinois Basin, including data from the St. Peter (red diamonds, this study), Eau Claire (green triangles, from Hyodo et al., 2014; Śliwiński et al., 2017), and Mt. Simon (blue circles, from Pollington et al., 2011, and this study) formations. Data clustering around 10‰ reflect analyses from detrital quartz grains (open symbols); values of $\delta^{18}O > 18$‰ are of diagenetic quartz overgrowths (filled symbols). Vertical black line is the predicted $\delta^{18}O$ value for quartz, if precipitated at 45 °C, in equilibrium with water ($\delta^{18}O = -3$‰). Vertical dotted black line is for quartz precipitated from $\delta^{18}O$(water) of 0% at 45 °C. Curved black line is $\delta^{18}O$(Qz) if temperature increases along a 30 °C/km geotherm, assuming $\delta^{18}O$(water) $= -3$‰, 1 km of erosion, and a surface temperature of 20 °C. Curved dotted line is the geotherm curve if $\delta^{18}O$(water) is held at 0%. (b) Difference in isotopic value between earliest quartz (detrital grain adjacent) overgrowth and other (later) overgrowth quartz analyses. DQ = detrital quartz, OQ = overgrowth quartz. (For interpretation of the references to colour in this figure legend, the reader is referred to the web version of this article.)

10‰ for $\delta^{13}C$), and steep gradients (up to 8‰ for $\delta^{18}O$ and up to 11‰ for $\delta^{13}C$ over <5 μm). This wealth of information would be lost by homogenization during sampling without the small spot capabilities of SIMS analysis correlated to SEM imaging and EPMA of cation compositions. Important generalizations can be made in spite of basin-wide variability. Quartz overgrowths formed after initial high-$\delta^{18}O$ dolomite cementation, and in many samples the majority of quartz overgrowths predate a peak in the Fe content of developing carbonate cements. The concentric zoning of $\delta^{18}O$ in individual quartz overgrowths formed mainly during pre-270 Ma burial. Post-quartz drops in $\delta^{18}O$ in carbonates are associated with increases in Fe; carbonates tend to have lower $\delta^{18}O$ and higher Fe towards the end of carbonate growth (Fig. 10a).

For the purposes of drawing comparisons between the diagenetic histories recorded by isotopic data from different cores, dolomite/ankerite analyses were divided into four different growth phases

correlatable based on the petrography and isotopic trends (Figs. 10, 11, also Figs. 3c, 5c, 6c). Phase 1 consists of the innermost portions of dolomite cements present in samples, which are nearly stoichiometric (Ca_{50}-Ca_{55}, Fe# < 0.05), and commonly surrounded by an irregular boundary, interpreted to represent a dissolution event. Basin-wide, Phase 1 carbonates vary from 21 to 27‰ in $\delta^{18}O$ and -1 to -7‰ range in $\delta^{13}C$. Phase 2 carbonates are the zoned low-$\delta^{18}O$ dolomite/ankerites that postdate the end-Phase 1 dissolution boundary, predate the most Fe-rich ankerites, and possess significantly lower $\delta^{18}O$ and similar $\delta^{13}C$ values when compared to Phase 1. Phase 3 carbonates correspond to the most Fe-rich band of ankeritic growth, and commonly show the most significant shifts in $\delta^{13}C$ to either higher or lower values, depending on the sample. Phase 4 dolomite/ankerites postdate Phase 3, and basinwide show less variability in $\delta^{13}C$ values than Phase 3. The majority of quartz overgrowths formed between Phases 1 and 3, and
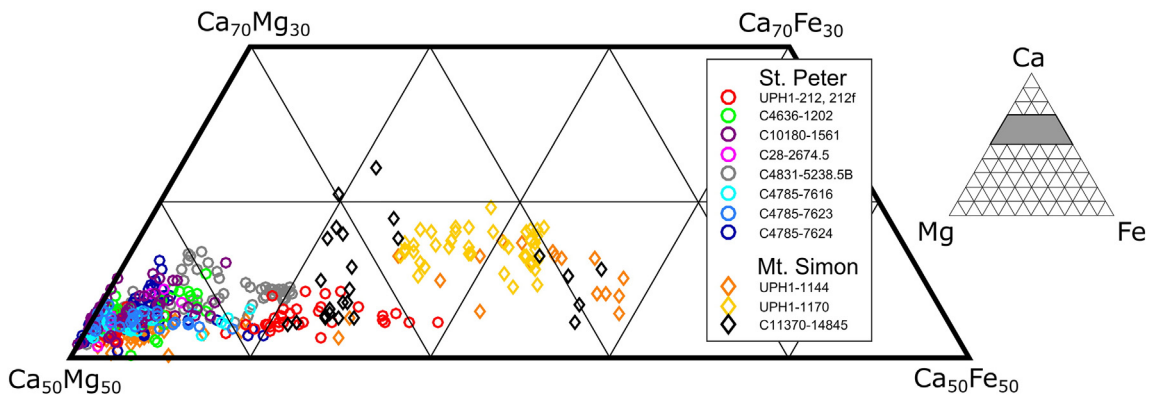
Fig. 9. Ca-Mg-Fe ternary plot for all analyzed dolomite/ankerites, colour-coded by sample number. Data are from both the St. Peter (circles) and Mt. Simon (diamonds) formations in the Illinois Basin. (For a color version of this figure, the reader is referred to the web version of this article.)
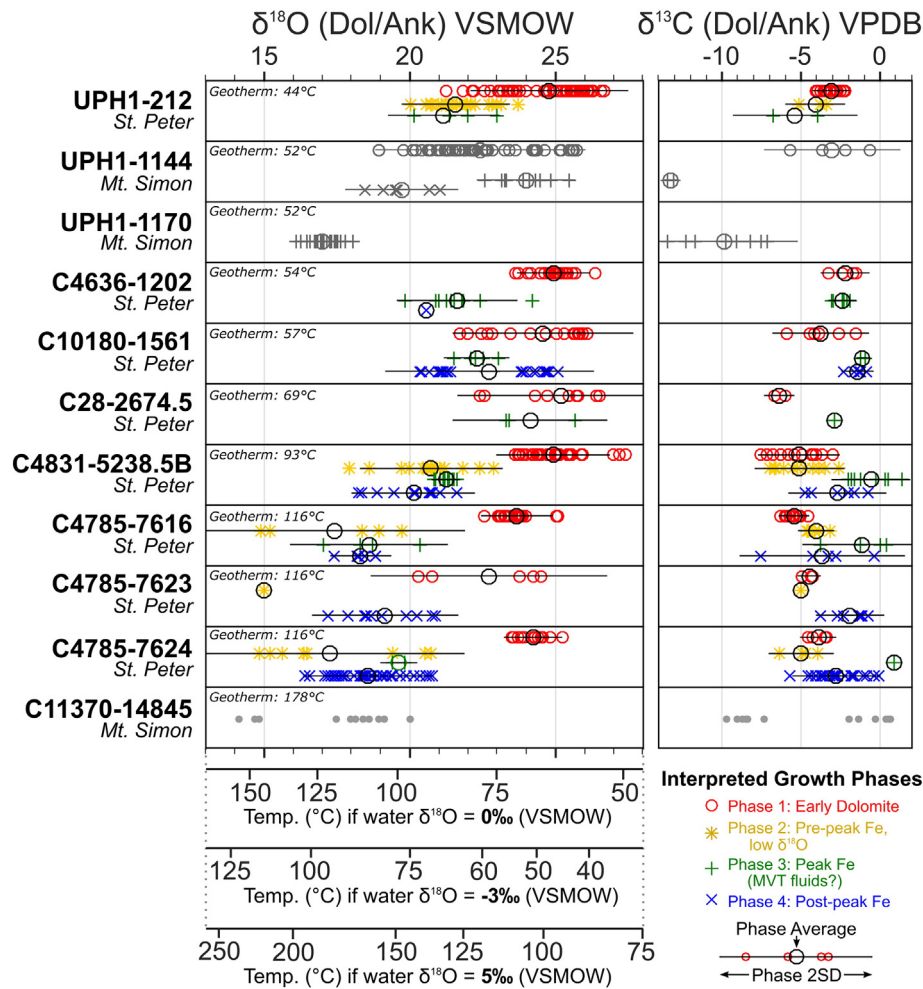
Fig. 10. Distributions of dolomite/ankerite $\delta^{18}O$ and $\delta^{13}C$ data from this study separated out by sample name and growth phase. St. Peter data are colour coded by growth phase, and Mt. Simon samples UPH1-1144, UPH1-1170, and C11370-14845 have been plotted with grey symbols to visually emphasize that they are a different formation. The average of each growth phase in a sample is denoted by a large black circle. Shown for reference below the $\delta^{18}O$ data are the calculated temperatures of dolomite formation for the cases in which dolomite precipitated from $\delta^{18}O_{(water)}$ of $-3‰$, $0‰$, and $5‰$. Geotherm temperatures were determined by assuming a surface temperature of 20 °C, a 30 °C/km geotherm, and a projected additional 1 km of overburden uniformly distributed across the basin. These temperatures represent the expected maximum temperatures each sample would have experienced in the absence of anomalous heating or MVT fluid flow. (For a color version of this figure, the reader is referred to the web version of this article.)

in some locations was concurrent with the growth of Phase 2 carbonate (Appendix E).

Earlier studies have presented a burial and heating model for precipitation of quartz overgrowths in the Illinois basin before the MVT event (Fig. 8b) that assumes: restricted flow of fluids during the compaction phase of burial, a constant value of $\delta^{18}O_{water} = -3‰$, a geothermal gradient of 30 °C/km, surface $T = 20$ °C, and 1 km of erosion and uplift (Pollington et al. 2011; Hyodo et al. 2014). If such a model is applied to $\delta^{18}O$ for the analyzed dolomites, there is good conformance at moderate depths (500–2500 m, cores C4831 and C4785) between estimated 30 °C/km geotherm temperatures and the lowest $\delta^{18}O$ values expected at those temperatures from aqueous fluids with $\delta^{18}O = -3‰$ (Fig. 10). However, if it is assumed that original fluid $\delta^{18}O$ values were closer to $-1‰$, as has been suggested from recent clumped isotope data (Came et al., 2007; Finnegan et al., 2011; Cummins et al., 2014), then the model deviates slightly from the data and requires that the geotherm be elevated above 30 °C/km, or that fluids evolved to heavier oxygen isotope compositions before maximum burial.

The deepest sample of Mt. Simon sandstone (C11370) doesn't extend to values as low as the 30 °C/km-geotherm estimate, possibly because cementing minerals grew to impingement before maximum depths of burial, or because $\delta^{18}O_{(water)}$ was elevated by the time maximum temperatures were reached. In contrast, many shallow samples plot lower in $\delta^{18}O$ than reasonable $\delta^{18}O_{(water)}$ values and geotherm

temperatures would suggest, an observation that has three potential explanations. 1) If the burial depths and amounts of uplift of the St. Peter and Mt. Simon sandstones are underestimated near the Wisconsin Arch, this would mean that rocks were buried to greater depths and exposed to higher temperatures than estimated in the model. 2) Alternatively, these low $\delta^{18}O(Dol/Ank)$ values might result from changes in the $\delta^{18}O$ of fluids and heating during the MVT event (Phase 3). These samples are closer to the UMV ore deposits than others located further into the basin, and the low $\delta^{18}O$ values might then reflect more localized regions of elevated temperature during brine migration. 3) These shallow low $\delta^{18}O$ cement phases formed under the influence of infiltrating low-$\delta^{18}O$ meteoric water during their growth.

In the following sections, more detailed analysis will be given of each of the diagenetic phases studied here in their approximate order of formation: Phase 1 Early Carbonates, Quartz Overgrowths, Phase 2 Pre-Peak Fe Carbonates, Phase 3 Peak-Fe Carbonates, and Phase 4 Post-Peak Fe Carbonates.

4.1. Early carbonates (innermost carbonate cements/carbonate growth Phase 1)

With the exception of UPH1-1170 and C11370-14845 from the Mt. Simon, all analyzed zoned dolomite/ankerites contain near-stoichiometric (Fig. 9) inner dolomite cements with variable $\delta^{18}O$,
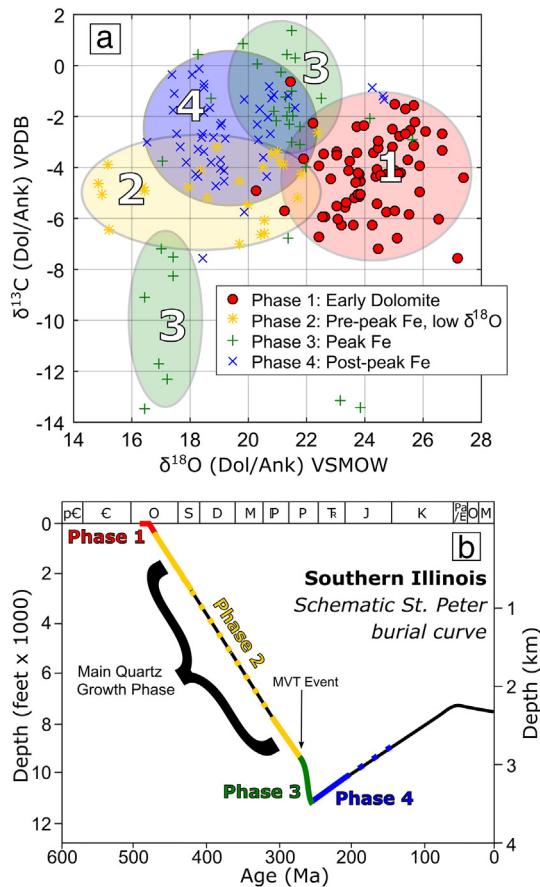
Fig. 11. (a) Cross plot of dolomite/ankerite δ^{18}O vs. δ^{13}C values, coded by growth phase, colored as in Fig. 10. Data are from both the St. Peter and Mt. Simon formations, and only plotted when δ^{18}O and δ^{13}C pits are closely correlatable from the same zone. With the exception of samples from core UPH1, all St. Peter sample Phase 3 carbonates plot high in δ^{13}C (δ^{13}C > −3‰). All Mt. Simon Phase 3 carbonates plot low (δ^{13}C < −7‰). For a detailed interpretation of these separate growth phases, see the text. (b) Schematic carbonate and quartz growth histories in the St. Peter formation of the Illinois Basin using the burial model of Pitman et al. (1997). (For a color version of this figure, the reader is referred to the web version of this article.)

from 22 to 27‰ (growth Phase 1, Fig. 11). There is good conformance between the range of these early dolomite δ^{18}O values and average values previously reported for dolomites in the overlying Platteville (24 to 26‰) (Hall and Friedman, 1969), the base of which was within a few meters for several of these samples. However, other samples (UPH1-212, UPH1-1144, C10180-1561) have relatively low δ^{18}O values (21 to 24‰) in the innermost dolomite, that are surrounded by bands of higher δ^{18}O dolomite (Figs. 3, 4a, 5).

Three possibilities for explaining these anomalously low early values are considered below. 1) These values are for carbonates that exchanged with unmodified seawater and directly reflect seawater δ^{18}O values. 2) These values reflect mixing of meteoric-water and seawater during the early stages of cementation. 3) The early cements were recrystallized, and the low δ^{18}O values reflect interaction with a later, hotter (or lower δ^{18}O) fluid.

Addressing the first possibility, precipitation from pristine seawater, although the zoning pattern of cements suggests that the inner carbonates formed first as primary low-δ^{18}O precipitates from seawater or an early connate derivative, there are two reasons to question such a simple explanation. First and foremost, if it is assumed that porewaters were not significantly different from estimates of Cambro-Ordovician seawater (δ^{18}O ≈ −3 to −1‰) (Came et al., 2007; Jaffrés et al., 2007; Cummins et al., 2014), such low δ^{18}O mineral values require temperatures >50 °C before initial burial, an unrealistic result for a tectonically inactive region. Because these dolomites all are petrographically

earlier than low-temperature quartz growth, it is unlikely that hotter geothermal fluids infiltrated these rocks at the time of initial dolomite formation. There is disagreement about the δ^{18}O value of Cambro-Ordovician seawater, and water may have been lower in δ^{18}O. However, a second piece of evidence argues against lower Cambro-Ordovician seawater δ^{18}O—there is also a sharp rise in δ^{18}O that occurs just outside the innermost zone of cement (in growth Phase 2, Figs. 3 and 5). This increase would be difficult to explain in the context of pristine seawater and shallowly buried sandy sediments, and is even more difficult to explain with a lower δ^{18}O of seawater. If Ordovician seawater was lower in δ^{18}O, then the later, higher δ^{18}O cements of Phase 1 would require lower temperatures or higher δ^{18}O fluid. However, diagenetic temperatures cannot have been significantly lower than seawater and it is unlikely that water-rock interaction significantly shifted porewater compositions to higher δ^{18}O at the time.

Addressing the second possibility, (meteoric/seawater mixing), if the early dolomites did not initially precipitate from seawater-like compositions and have not recrystallized, then they likely originated in the seawater/meteoric water-mixing zone. A number of models for low temperature dolomite formation invoke coastal settings, where low-δ^{18}O meteoric fluids can mix with seawater in pore fluids and lower the δ^{18}O below that of the ocean (for a review of dolomite precipitation models, see Warren, 2000). Some studies have proposed that mixing connate fluids with meteoric water can be a direct cause of dolomite precipitation (Hanshaw et al., 1971; Badiozamani, 1973; Folk and Land, 1975), although more recently the invocation of this process to explain pervasively dolomitized limestones has been criticized on the basis that kinetic rather than equilibrium processes control dolomite precipitation, and because there are no known examples of massive dolostones actively forming in modern depositional settings (Machel and Mountjoy, 1986; Hardie, 1987; Machel, 2004; Melim et al., 2004). Whatever the origin, dolomite mineral nucleation is well documented in low-temperature coastal settings, demonstrating that dolomite nucleation near the ocean/meteoric water boundary is possible in modern environments and likely in the past (Ward and Halley, 1985; Randazzo and Cook, 1987; Cander, 1994; Humphrey, 2000). In the Illinois Basin, subsequent to the lower δ^{18}O inner dolomite cement (20 to 24‰), δ^{18}O values in several samples rise to 25–27‰, values more consistent with precipitation from low temperature seawater, which would be expected as meteoric water recedes during transgression. In the modern day, it would be reasonable to observe annual averaged rainwater δ^{18}O values of ~− 7 to −9‰ along the western equatorial margins of continents (Bowen, 2010); thus, it is not unreasonable to assume that meteoric fluids in Cambrian-Ordovician Illinois might have achieved a similar magnitude of deviation from seawater.

The third possible explanation for the low δ^{18}O inner carbonate cements of Phase 1 is that they formed by recrystallization of metastable dolomite, and thus record values that are younger than the original cement. Low temperature calcian-dolomite often precipitates as a metastable precursor, and recrystallizes with X(Ca) closer to stoichiometric dolomite over time. This process has been proposed in dolomite-rich rocks to explain a wide range of potentially covariant trends, including crystal size, mol% Ca, δ^{18}O, δ^{13}C, Sr, Mn, Na, and ^{87}Sr/^{86}Sr ratios (Malone et al., 1994; Al-Aasm, 2000; Rott and Qing, 2013; Kaczmarek and Sibley, 2014). The recrystallization to stoichiometric dolomite compositions can be gradual and take tens or even hundreds of millions of years, and unmetamorphosed Paleozoic dolomites can retain non-stoichiometric Ca/(Mg + Fe) ratios (Land, 1985). Evidence suggests that highly unstable precursors (~60 mol% CaCO$_3$) can be expected to undergo noticeable recrystallization in <1000 years especially when exposed to fluids and elevated temperatures (Gregg et al., 1992; Malone et al., 1996). If the Phase 1 dolomite cements in this study were still somewhat metastable and prone to selective recrystallization at the time of the MVT hydrothermal fluid activity, then recrystallization at high temperature (MVT fluids at >100 °C) and/or different fluid conditions could have produced new inner dolomite cements (Phase 1)

lower in $\delta^{18}O$ than the precursor metastable phase, as has been observed in recrystallizing dolomites in other terranes (Reinhold, 1998; Rott and Qing, 2013). Values of $\delta^{13}C$ would be less susceptible to change during this process than $\delta^{18}O$ due to the low C/O ratios of groundwater compared to carbonate, and thus $\delta^{13}C$ has greater fidelity as a record of pre-recrystallization dolomite isotopic compositions (Kupecz et al., 1993). BSE and CL imaging of the innermost dolomite in the Phase 1 cements sometimes shows irregular boundaries between patchy regions of differing Fe contents (e.g., Figs. 3a, 5a), consistent with recrystallization, but if recrystallization occured early, it is possible that low-$\delta^{18}O$ meteoric water caused these low $\delta^{18}O$ dolomites. If metastable Ca-rich dolomites originally existed in these samples, they have recrystallized and are indistinguishable from most subsequent cement phases on the basis of Ca/(Ca + Mg + Fe) values alone, falling in the 50–55 mol% $CaCO_3$ range.

It is significant that not all samples possess anomalously low $\delta^{18}O$ cores, which indicates that the process creating them is not acting universally across the basin. Because of this heterogeneity, and given our current understanding of the propensity of dolomite to form in mixing zones (Warren, 2000), the meteoric/seawater interaction explanation seems the most likely.

4.2. Quartz overgrowths

The ranges of $\delta^{18}O$ and zoning of $\delta^{18}O$ within individual quartz overgrowths are similar to those reported by previous authors for the Illinois Basin (Pollington et al., 2011; Hyodo et al., 2014). In most samples, the early quartz in an overgrowth has the highest $\delta^{18}O$ nearest to the detrital grain boundary and then $\delta^{18}O$ steadily drops in value towards the rim. This trend is consistent with the model of burial-driven compaction, pressure solution, and heating of sandstone containing relatively immobile Paleozoic seawater as proposed by Pollington et al. (2011).

In many of the analyzed samples, the early Phase 1 carbonates grew before quartz overgrowths and the late carbonates (growth Phases 3 and 4) grew after the quartz overgrowths (Appendix E). It should be emphasized that this does not necessarily equate to a hiatus in carbonate growth in all samples, but that quartz growth rates, if concurrent with carbonate cementation, were higher than carbonate cementation rates during this period. This carbonate-quartz carbonate alternation in diagenetic growth history has been observed by others in the Paleozoic sands of the Illinois Basin (Pitman and Spötl, 1996; Fishman, 1997; Pitman et al., 1997), and therefore likely reflects long-term basin-wide shifts in water chemistry. Presumably, late carbonates developed after conditions become less favorable for quartz growth (i.e., a cessation of burial and pressure solution) and more favorable to carbonate growth (in many samples late carbonates are interpreted to mark the start of the MVT fluid flow event, which post-dates major periods of sediment deposition in the Illinois Basin). One additional feature to these overall quartz trends is seen in C4785–7624, where quartz overgrowths reach a minimum $\delta^{18}O$ of around 19‰ and then show a late return to higher values (~24‰, Appendix D). Such late values were also reported in a few samples by Hyodo et al. (2014) who suggested that they may reflect a late cooling or local growth of quartz exposed to higher $\delta^{18}O$ fluids associated with the MVT event.

4.3. Pre-peak Fe carbonates (carbonate growth Phase 2)

Moving outwards from the innermost portion of each zoned dolomite/ankerite cement, $\delta^{18}O$ values tend to fall as Fe content in the carbonate rises. Surrounding Phase 1 dolomites, but prior to the growth of the most ankeritic compositions (Phase 3), some of the samples show dissolution boundaries associated with sharp drops in mineral $\delta^{18}O$ values. In samples C4831-5238.5 and C4785, these transitions are quite large and $\delta^{18}O$ changes by up to 8‰. In contrast, $\delta^{13}C$ values do not change significantly from Phase 1 to 2 (Fig. 11a). The presence of

the dissolution surface at the end of Phase 1 implies that portions of the intervening record were lost, and may be interpreted one of two ways. If Phase 1 carbonates preserve the earliest growth, then the drop in carbonate $\delta^{18}O$ from Phase 1 to 2 requires either a significant rise in temperature (assuming a constant $\delta^{18}O_{porewater}$) during the carbonate hiatus, or a large negative shift in $\delta^{18}O_{porewater}$ values. Incursion of meteoric water is commonly seen in shallow aquifers and may provide an explanation for low $\delta^{18}O$ values present in the latter part of growth Phase 2 in UPH1-212, which would have been near the northern margin of the basin and comparatively shallow relative to deeper samples (~1 ± 0.5 km for shallow northern Illinois rocks) (Rowan et al., 2002; Makowitz et al., 2006). Incursion of meteoric water is deemed unlikely as a factor for deeper cements, however.

If Phase 2 cements record precipitation from porewaters not significantly altered in $\delta^{18}O$ from −3 to −1‰ (Cambro-Ordovician seawater), then the carbonates of this growth phase record $\delta^{18}O$ values that are fairly consistent with estimated maximum burial temperatures for C4831 (~95 °C) and C4785 (~115 °C). It is significant that Phase 2 contains the lowest $\delta^{18}O$ values measured in either C4831 or C4785, such that later carbonate phases (Phases 3 and 4) must have been formed after either temperatures drop (which would be surprising before exhumation in the Illinois Basin), or after waters rose to higher $\delta^{18}O$ values. The latter scenario is more likely; MVT fluids would have caused significant water-rock interaction along their flowpath, and even modern waters of the Illinois Basin have elevated $\delta^{18}O$ values due to more prolonged water-rock interaction (Clayton et al., 1966).

A second period of carbonate-dominated growth, after the prolonged period of burial and compaction when quartz growth was dominant, would require a renewed source of carbonate ions and possibly a change in pH, implying changes in fluid composition. Because this transition back to carbonate growth is seen in multiple samples, the most likely time for Phase 2 carbonates to grow would be before or at the onset of MVT fluid movement, when changes in fluid composition and pH were likely small and still relatively local. In any case, the source of carbonate ions for the dolomite/ankerites precipitating in these siliciclastic units after burial was likely adjacent units, and dolomite/ankerite precipitation after the rock was isolated from seawater would have required the significant movement, probably gravity-driven, of fluid through adjacent units.

4.4. Peak-Fe carbonates, MVT-related (carbonate growth Phase 3)

After Phases 1 and 2, Fe content in carbonate consistently shows a sharp and dramatic increase in Fe#, hereafter referred to as Phase 3 or "peak-Fe" carbonates. Coincident with this carbonate phase, $\delta^{13}C$ becomes more variable (e.g., Fig. 7c,d). For the same reasons previously discussed for growth Phase 2, it is considered unlikely that low-$\delta^{18}O$ fluids of meteoric origin significantly interacted with the carbonates after quartz overgrowths began to develop. If there was no potential source of low-$\delta^{18}O$ fluids at the time, then the observed decline in $\delta^{18}O$ values leading into growth Phase 3 must reflect a significant rise in temperature during burial and possibly MVT fluid passage. Fluid inclusion data in the Mt. Simon and St. Peter formation cements show that temperatures were elevated above the geotherm at some point in their history (Fishman, 1997; Chen, 2001), but the timing of inclusion formation is not well constrained. Temperatures during the MVT event are modeled on the north side of the basin to have been generally higher than the geotherm at all depths due to heating by migrating fluids (Bethke and Marshak, 1990; Arnold et al., 1997; Rowan et al., 2002).

During a period of major fluid flow, it cannot be assumed that temperatures follow the equilibrium geothermal gradient, or that porewaters have the isotopic composition of original formation water; such events tend to promote water-rock interaction, affecting fluid chemistry. Thus, the shallow samples (UPH1, C4636, C10180) with Fe-rich Phase 3 carbonates too low in $\delta^{18}O$ to have precipitated from fluids with $\delta^{18}O = -3‰$ are strong evidence for Phase 3 precipitation during

the MVT event when temperatures would have been elevated. These samples plot lower in $\delta^{18}O$ than an estimated 30 °C/km gradient and $\delta^{18}O_{porewater} = -3‰$ (<500 m, Fig. 10), likely due to the elevated temperature at shallow depths. In contrast, Phase 3 carbonates from samples at present depths >500 m (cores C4831 and C4785) plot higher in $\delta^{18}O$ than Phase 2 carbonates (Fig. 10). If hot MVT brines were sourced from deeper in the basin, they could possess $\delta^{18}O$ values of 1.5‰ to 5.7‰ that were observed in fluid inclusions by McLimans (1977) in UMV fluid inclusions. Higher $\delta^{18}O$ fluids would precipitate ankerite with higher $\delta^{18}O$ values.

If the peak-Fe carbonate growth phase (Phase 3) formed during the MVT event, then the $\delta^{18}O$ of fluids that migrated updip along the northern slope of the basin was likely positive during this time. As a point of reference, +3‰ water precipitating UPH1 ankerites at the northern end of the Illinois Basin would require temperatures as high as 120 °C in the St. Peter (ankerite $\delta^{18}O$ ~ 20‰) and 155 °C (assuming +3‰ water) further down UPH1 in the Mt. Simon (ankerite $\delta^{18}O$ ~ 17‰). Assuming the same $\delta^{18}O_{(water)} = +3‰$ values for C4785 ankerite yields temperatures as high as 180 °C in the St. Peter in south-central Illinois (modern depth ≈ 2.3 km, $\delta^{18}O_{Ank}$ ~ 15‰). The range in $\delta^{18}O$ within the Fe-rich zone (Phase 3) is interpreted to be a reflection of both temperature and fluid composition. Samples that were exposed to hotter fluids (those buried more deeply or in more direct communication with the primary MVT fluid-flow conduit of the Mt. Simon formation) tend to record lower $\delta^{18}O$ values.

Values of $\delta^{13}C$ in carbonate show a strong sensitivity to carbon source, as there is less of a temperature effect on the fractionation of carbon isotopes than in the oxygen system (Friedman and O'Neil, 1977; Horita, 2014). The range in $\delta^{13}C$ values seen in Phase 3 is interpreted to primarily reflect two different sources of carbon, carbonate (high $\delta^{13}C$, source ~ 0‰) or thermal maturation of organic matter (low $\delta^{13}C$, source < −25‰). Mt. Simon samples collected from core UPH1 (1170) near the UMV ore district contain Fe-rich ankerites that drop to $\delta^{18}O$ values of around 17‰ and $\delta^{13}C$ values as low as −13‰. Negative carbon excursions are seen in association with the Fe-rich band in core UPH1, in both the St. Peter (Fig. 3) and the Mt. Simon (Appendix C). UPH1 rocks were never buried deeply enough in Wisconsin to provide an explanation for these post quartz overgrowth, negative $\delta^{13}C$ excursions without invoking hot migrating fluids, or some other nonmarine fluid pulse of anomalous origin. Similarly, bulk analyses of calcites related to the UMV-MVT-ores show excursions to values as low as 17‰ for $\delta^{18}O$ and −12.5‰ for $\delta^{13}C$ (McLimans, 1977). These similarities in the magnitude of negative $\delta^{13}C$ shifts in both UMV calcites and UPH1 St. Peter carbonates do not necessarily mean that the fluids experienced in both the UMV district outcrops and nearby drillcore were identical, but the magnitudes of the excursions in both $\delta^{13}C$ and $\delta^{18}O$ are similarly large and in the same direction, consistent with recording different portions of the same event. Hot MVT fluids in the Mt. Simon formation (perhaps in excess of 150 °C, Bethke, 1986; Rowan et al., 2002) are likely to have interacted with organic carbon at some point along their flowpath (possibly along the overlying Eau Claire or even within intermittent thin shale beds in the Mt. Simon itself) during migration, and carbonates that precipitated from a higher percentage of these fluids should have more negative carbon values (Mt. Simon samples and some St. Peter samples, e.g., UPH1-1170, UPH1-212). Even invoking late hot fluids in UPH1-212, though, the $\delta^{13}C$ range present in the two Mt. Simon samples analyzed from the same core (down to −13‰) are more negative than that found in the St. Peter (down to −8‰, Fig. 10), suggesting fluids in the Mt. Simon experienced a lower proportion of exchange with carbonate than fluids in the St. Peter.

However, if hot MVT fluids interacted with large volumes of limestone or dolostone (or there was a relative lack of organic carbon), then it is a common observation for $\delta^{13}C$ values to approach the values of marine carbonate. The St. Peter is underlain by the thick carbonate sequence of the Prairie du Chien Group, which could have been the source of carbon. This would explain the high $\delta^{13}C$ excursions seen in

parts of the St. Peter coincident with the sharp drop of $\delta^{18}O$ associated with the MVT (e.g., C4831-5238.5, C4785-7624; i.e., boundary 7 in Fig. 6, boundary 5 in Fig. 7; again, these zones are used for intra-sample correlation, not inter-sample correlation). In the vicinity of the UMV, the St. Peter has filled paleovalleys in the underlying unconformity surface that incise and in places eroded completely through the underlying Prairie du Chien carbonates. These sandstones are interpreted to have been fluid pathways for upwards flow that allowed MVT fluids to cut through of the intervening low-permeability strata (Mai and Dott, 1985). This bypassing of comparatively high $\delta^{13}C$ carbonate units potentially explains the observed low $\delta^{13}C$ trends in these late cements.

4.5. Post peak-Fe carbonates (carbonate growth Phase 4)

After peak-Fe, there is typically a final stage of carbonate growth where Fe content is diminished and the $\delta^{13}C$ shifts seen during Phase 3 growth begin to trend back towards values present prior to the peak in Fe#. The source of carbon for the dolomite and ankerite precipitated in these siliciclastic units after burial was likely adjacent units, and the movement of fluids through adjacent units, under favorable conditions, would encourage faster precipitation rates by increasing the rate of supply of carbonate ions to these growing cements. As the fluid flow event (likely MVT) that produced the peak-Fe Phase 3 carbonates began to wane, then the precipitation of carbonate cements might have waned as well. The zoned dolomite/ankerite cements that developed after peak-Fe are interpreted to correspond to this final phase and capture a return to conditions more similar to those prior to the MVT. In deep samples, this manifests itself as continued low $\delta^{18}O$ values not significantly different from those during peak-Fe (temperature remains elevated), while $\delta^{13}C$ trends towards values that were present prior to peak-Fe (equilibrating with the local mineralogic environment).

5. Perspectives

Throughout the geologic record, carbonate minerals are considered to possess some of the most direct records of oceanic and atmospheric histories. However, they are also particularly susceptible to low temperature alteration processes and fluid-rock interaction. Notably, none of the carbonates studied in this paper are interpreted, based on geochemical and petrographic observations, to have formed in direct contact with seawater, and therefore formed in a purely diagenetic regime. Evidence of diagenesis is ubiquitous in the sedimentary record, and yet it remains poorly understood. Improvements in the ability to qualify, quantify, and predict the timing and bulk geochemical effects of diagenesis in sedimentary rock will inevitably improve the accuracy of interpretations of sedimentary histories.

SEM/SIMS provides a powerful tool with which to interrogate diagenetic cements, as single diagenetic carbonate minerals can contain micron-scale $\delta^{18}O$ and $\delta^{13}C$ records of surprising complexity. With this realization come opportunities for new approaches to old diagenetic problems, such as interrogating water-sediment interactions in Holocene environments, or reexamining the fidelity of Precambrian stable isotope record and proposed secular trends in carbonate-rich units by separating them from diagenetic overprinting. Similar features to those discussed in this paper will probably be found as these approaches are applied in other localities; however, the interpretations of such results are in their infancy and will be greatly enhanced if temperatures can be estimated for individual growth bands that have been isotopically analyzed by SIMS. Distinguishing broad basin-wide trends from the details of local geology will be the subject of many future studies. Perhaps, as understanding of these systems continues to evolve, a point will be reached where confident interpretation of the fluid history of a relatively unstudied basin may be made from a few key cemented samples.
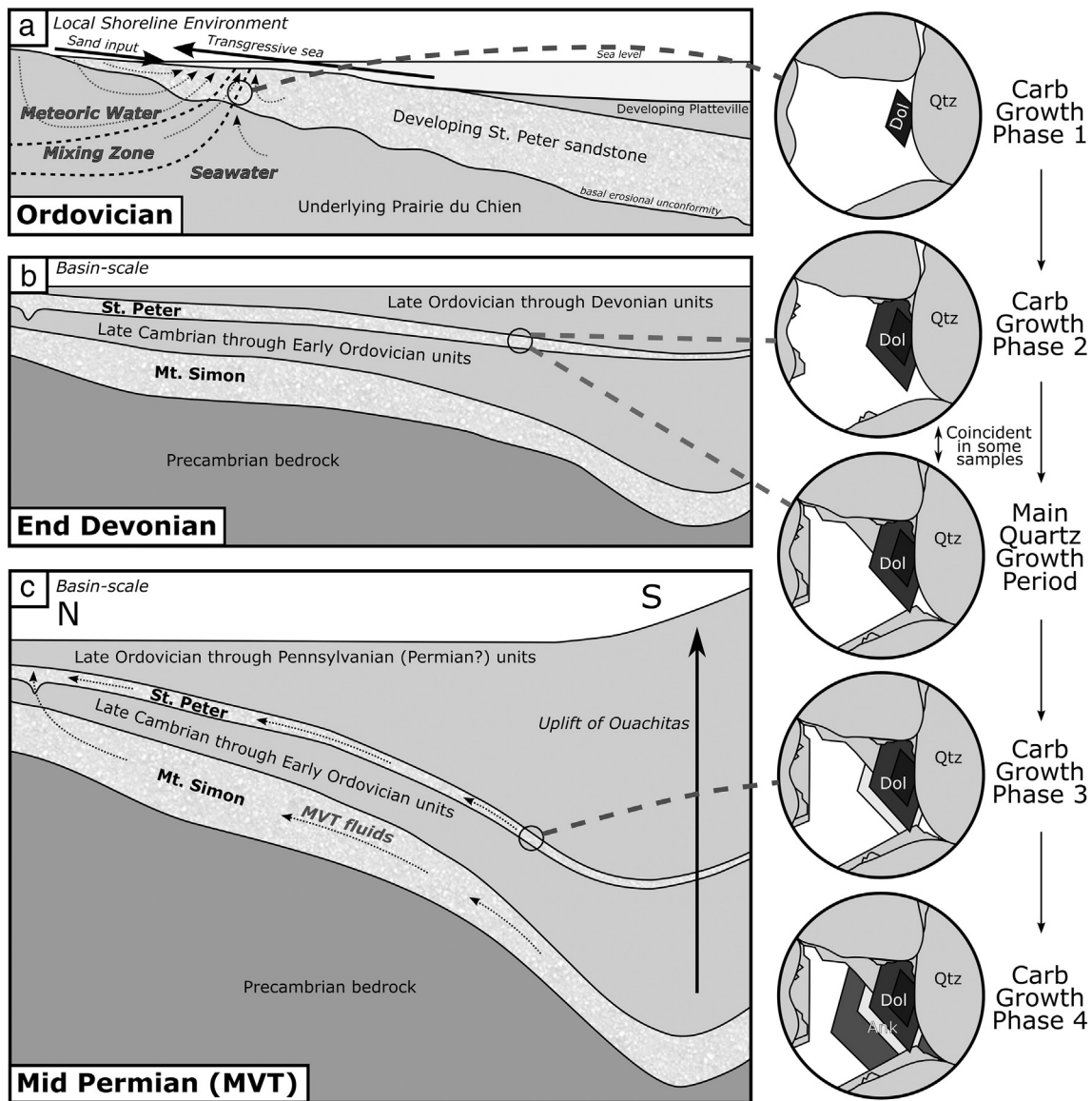
Fig. 12. Hypothesized relations between Illinois Basin sandstone burial evolution and the sequential development of diagenetic quartz and carbonate cements in the St. Peter sandstone. (a) Shoreline environment in which sands are deposited upon an erosional surface on the Prairie du Chien group. As the ocean transgresses, the sands are buried beneath the Platteville limestone (St. Peter). Growth Phase 1 comprises the innermost portions of dolomite cements, which were one of the first diagenetic minerals to develop and may have nucleated in the meteoric-seawater mixing zone. (b) Transgression gradually removes the meteoric influence, and growth Phase 2 comprises early burial carbonate and minor quartz overgrowths from a seawater-derived connate fluid. The main quartz growth phase occurs as basinwide burial progresses and diagenetic carbonate formation wanes in the absence of major fluid flow or an alternate source of carbonate ions, but pulses of carbonate Phase 2 growth are still possible. (c) Growth Phase 3 occurs as warm MVT fluids pass through the siliciclastic units of the basin. Growth Phase 4 occurs post-MVT.

6. Conclusions

A detailed chronology of thermal and fluid events is recorded by diagenetic cements in the Mt. Simon and St. Peter sandstones of the Illinois Basin. The SEM/SIMS approach combines SEM-based petrography and in situ stable isotope analysis by SIMS, and reveals this record in greater detail than has previously been possible for any sedimentary basin. This richness of information was previously unrecognized and reveals large isotopic variability (up to 10‰ for $\delta^{13}C$ in dolomite/ankerite and up to 10‰ for $\delta^{18}O$ in dolomite/ankerite and quartz) within small (<100 μm) cements, demonstrating the importance of this new approach for studying carbonate diagenesis. Diagenetic carbonates in the Illinois Basin preserve evidence of a complex history in their isotopic records, including 1) early mixing zone cements, 2) cements that formed during burial and heating with low fluid-flow rates controlled by compaction, and 3) cements formed during faster MVT-related gravity-driven fluid flow (Fig. 12). Hot MVT fluids appear to have

imprinted a basinwide signal in these cements, with $\delta^{13}C$ values influenced by assimilation of organic carbon from shales and exchange with carbonate-rich units. Quartz overgrowths in sandstone formed in the prolonged period of burial, pressure solution and compaction (Cambrian to Permian), whereas carbonate cements in these sandstones bracket quartz, offering clues to initial burial conditions and capturing later periods of punctuated fluid flow.

collected from drill core held at the Illinois State Geological Survey and the Wisconsin Geological & Natural History Survey. We thank Bob Mumm at the ISGS, and Patrick McLaughlin and Jay Zambito at the WGNHS, for their assistance in locating samples. QGIS, Matlab, and the Microsoft Office suite provided invaluable tools for processing and displaying the data contained herein. WiscSIMS is supported by the U.S. National Science Foundation (EAR-1355590) and the University of Wisconsin-Madison.

Appendix A. Supplementary data

Supplementary data to this article can be found online at https://doi.org/10.1016/j.sedgeo.2017.09.004.

References

Al-Aasm, I.S., 2000. Chemical and isotopic constraints for recrystallization of sedimentary dolomites from the western Canada Sedimentary Basin. Aquat. Geochem. 6:227–248. https://doi.org/10.1023/A:1009611224589.

Arnold, B.W., Bahr, J.M., Fantucci, R., 1997. Paleohydrogeology of the Upper Mississippi Valley zinc-lead district. In: Sangster, D.F. (Ed.), Society of Economic Geologists Special Publication. 4. Data Reproductions Corporation, Autumn Hills, MI, United States (USA), pp. 378–389.

Badiozamani, K., 1973. The Dorag Dolomitization model, application to the Middle Ordovician of Wisconsin. J. Sediment. Petrol. 43:965–984. https://doi.org.ezproxy.library.wisc.edu https://doi.org/10.1306/74D728C9-2B21-11D7-8648000102C1865D.

Barnes, H.L., Lavery, N.G., 1977. Use of primary dispersion for exploration of Mississippi Valley-type deposits. Journal of Geochemical Exploration, Proceedings of the Sixth International Geochemical Exploration Symposium 8:105–115. https://doi.org/10.1016/0375-6742(77)90046-2.

Benson, M.E., Wilson, A.B., Bleiwas, D.I., 2015. Frac sand in the United States: a geological and industry overview (USGS numbered series No. 2015-1107). Open-File Report. United States Geological Survey, Reston, VA, United States (USA).

Berger, P.M., Roy, W.R., Mehnert, E., 2009. Geochemical modeling of carbon sequestration, MMV, and EOR in the Illinois Basin. Energy Procedia 1, 3437–3444.

Bethke, C.M., 1986. Hydrologic constraints on the genesis of the Upper Mississippi Valley Mineral District from Illinois Basin Brines. Econ. Geol. 81, 233–249.

Bethke, C.M., Marshak, S., 1990. Brine migrations across North America-the plate tectonics of groundwater. Annu. Rev. Earth Planet. Sci. 18, 287–315.

Bowen, G.J., 2010. Isoscapes: spatial pattern in isotopic biogeochemistry. Annu. Rev. Earth Planet. Sci. 38:161–187. https://doi.org/10.1146/annurev-earth-040809-152429.

Bowen, B.B., Ochoa, R.I., Wilkens, N.D., Brophy, J., Lovell, T.R., Fischietto, N., Medina, C.R., Rupp, J.A., 2011. Depositional and diagenetic variability within the Cambrian Mount Simon Sandstone: implications for carbon dioxide sequestration. Environ. Geosci. 18, 69–89.

Brannon, J.C., Podosek, F.A., McLimans, R.K., 1992. Alleghenian age of the Upper Mississippi Valley zinc–lead deposit determined by Rb–Sr dating of sphalerite. Nature 356: 509–511. https://doi.org/10.1038/356509a0.

Came, R.E., Eiler, J.M., Veizer, J., Azmy, K., Brand, U., Weidman, C.R., 2007. Coupling of surface temperatures and atmospheric CO2 concentrations during the Palaeozoic era. Nature 449:198–201. https://doi.org/10.1038/nature06085.

Cander, H.S., 1994. An example of mixing-zone dolomite, Middle Eocene Avon Park Formation, Floridan aquifer system. J. Sediment. Res. 64, 615–629.

Chang, L.L.Y., Howie, R.A., Zussman, J., 1996. Rock-forming Minerals, v. 5B: Non-silicates: Sulphates, Carbonates, Phosphates and Halides. 2nd ed. Longman Group, London.

Chen, Z., 2001. Diagenesis of Upper Cambrian Mount Simon Sandstone in the Illinois Basin; Microscale Investigation of Basinal Fluid Migration and Mass Transfer. Ph.D. Thesis. University of Tennessee at Knoxville, Knoxville, TN, United States (USA).

Chen, Z., Riciputi, L.R., Mora, C.I., Fishman, N.S., 2001. Regional fluid migration in the Illinois Basin: evidence from in situ oxygen isotope analysis of authigenic K-feldspar and quartz from the Mount Simon Sandstone. Geology 29, 1067–1070.

Clayton, R.N., Friedman, I., Graf, D.L., Mayeda, T.K., Meents, W.F., Shimp, N.F., 1966. The origin of saline formation waters: 1. Isotopic composition. J. Geophys. Res. 71, 3869–3882.

Clayton, R.N., O'Neil, J.R., Mayeda, T.K., 1972. Oxygen isotope exchange between quartz and water. J. Geophys. Res. 77:3057–3067. https://doi.org/10.1029/JB077i017p03057.

Coplen, T.B., Kendall, C., Hopple, J., 1983. Comparison of stable isotope reference samples. Nature 302:236–238. https://doi.org/10.1038/302236a0.

Cummins, R.C., Finnegan, S., Fike, D.A., Eiler, J.M., Fischer, W.W., 2014. Carbonate clumped isotope constraints on Silurian ocean temperature and seawater δ18O. Geochim. Cosmochim. Acta 140:241–258. https://doi.org/10.1016/j.gca.2014.05.024.

Dake, C.L., 1921. The problem of the St. Peter Sandstone. Columbia University, New York. Bulletin of the Missouri School of Mines. Technical Series 6(1), pp. 1–228.

Damberger, H.H., 1971. Coalification pattern of the Illinois Basin. Econ. Geol. Bull. Soc. Econ. Geol. 66:488–494. http://dx.doi.org.ezproxy.library.wisc.edu http://dx.doi.org/10.2113/gsecongeo.66.3.488.

Driese, S.G., Byers, C.W., Dott, R.H., 1981. Tidal deposition in the basal Upper Cambrian Mt. Simon Formation in Wisconsin. J. Sediment. Petrol. 51, 367.

Dwyer, S.E., 2011. Subsurface Dolomitization and Porosity Occlusion within Early to Middle Ordovician Strata of the Illinois Basin, USA. M.S. Thesis. University of Illinois at Urbana-Champaign, Urbana-Champaign, IL, United States (USA).

Eiler, J.M., Graham, C., Valley, J.W., 1997. SIMS analysis of oxygen isotopes: matrix effects in complex minerals and glasses. Chem. Geol. 138, 221–244.

Finnegan, S., Bergmann, K., Eiler, J.M., Jones, D.S., Fike, D.A., Eisenman, I., Hughes, N.C., Tripati, A.K., Fischer, W.W., 2011. The magnitude and duration of Late Ordovician–Early Silurian glaciation. Science 331:903–906. https://doi.org/10.1126/science.1200803.

Fishman, N.S., 1997. Basin-wide fluid movement in a Cambrian Paleoaquifer: evidence from the Mt. Simon Sandstone, Illinois and Indiana. In: Montañez, I.P., Gregg, J.M., Shelton, K.L. (Eds.), Basin-Wide Diagenetic Patterns: Integrated Petrologic, Geochemical, and Hydrologic Considerations. Special Publication 47. SEPM, Tulsa, OK, United States (USA), pp. 221–234.

Folk, R.L., Land, L.S., 1975. Mg/Ca ratio and salinity: two controls over crystallization of dolomite. Am. Assoc. Pet. Geol. Bull. 59, 60–68.

Friedman, I., O'Neil, J.R., 1977. Chapter KK. Chapter KK. Compilation of Stable Isotope Fractionation Factors of Geochemical Interest. In: Fleischer, M. (Ed.), Data of Geochemistry, United States Geological Survey Professional Paper 440-KK. United States Government Printing Office, Washington, DC, United States (USA), pp. 1–12.

Gharrabi, M., Velde, B., Sagon, J.P., 1995. Clay mineral evolution in the Illinois Basin and its causes. Clay Miner. 30, 353–364.

Gize, A.P., 1984. The Organic Geochemistry of three Mississippi Valley-Type ore Deposits. Ph.D. Thesis. Pennsylvania State University, State College, PA, United States (USA).

Gregg, J.M., Howard, S.A., Mazzullo, S.J., 1992. Early diagenetic recrystallization of Holocene (<3000 years old) peritidal dolomites, Ambergris Cay, Belize. Sedimentology 39:143–160. https://doi.org/10.1111/j.1365-3091.1992.tb01027.x.

Hall, W.E., Friedman, I., 1969. Oxygen and carbon isotopic composition of ore and host rock of selected Mississippi Valley deposits. United States Geological Survey, Professional Paper 650–C, pp. C140–C148.

Hanshaw, B.B., Back, W., Deike, R.G., 1971. A geochemical hypothesis for dolomitization by ground water. Econ. Geol. 66, 710–724.

Hardie, L.A., 1987. Perspectives: dolomitization: a critical view of some current views. J. Sediment. Res. 57, 166–183.

Hatch, J.R., Heyl, A.V., King, J.D., 1986. Organic geochemistry of hydrothermal alteration, basal shale and limestone beds, Middle Ordovician Quimbys Mill Member, Platteville Formation, Thompson-Temperly zinc-lead mine, Lafayette County, Wisconsin. In: Dean, W.E. (Ed.), Organics and Ore Deposits: Denver Regional Exploration Geologists Society Proceedings, Denver, CO, United States (USA), pp. 93–104.

Hervig, R.L., Williams, P., Thomas, R.M., Schauer, S.N., Steele, I.M., 1992. Microanalysis of oxygen isotopes in insulators by secondary ion mass spectrometry. Int. J. Mass Spectrom. Ion Process. 120:45–63. https://doi.org/10.1016/0168-1176(92)80051-2.

Hoholick, J.D., Metarko, T., Potter, P.E., 1984. Regional variations of porosity and cement; St. Peter and Mount Simon sandstones in Illinois Basin. Am. Assoc. Pet. Geol. Bull. 68, 753–764.

Horita, J., 2014. Oxygen and carbon isotope fractionation in the system dolomite–water–CO2 to elevated temperatures. Geochim. Cosmochim. Acta 129:111–124. https://doi.org/10.1016/j.gca.2013.12.027.

Humphrey, J.D., 2000. New geochemical support for mixing-zone Dolomitization at Golden Grove, Barbados. J. Sediment. Res. 70, 1160–1170.

Hyodo, A., Kozdon, R., Pollington, A.D., Valley, J.W., 2014. Evolution of quartz cementation and burial history of the Eau Claire Formation based on in situ oxygen isotope analysis of quartz overgrowths. Chem. Geol. 384:168–180. https://doi.org/10.1016/j.chemgeo.2014.06.021.

Jaffrés, J.B., Shields, G.A., Wallmann, K., 2007. The oxygen isotope evolution of seawater: a critical review of a long-standing controversy and an improved geological water cycle model for the past 3.4 billion years. Earth Sci. Rev. 83, 83–122.

Johnson, C.M., Winter, B.L., 1999. Provenance analysis of lower Paleozoic cratonic quartz arenites of the North American midcontinent region: U-Pb and Sm-Nd isotope geochemistry. Geol. Soc. Am. Bull. 111, 1723–1738.

Kaczmarek, S.E., Sibley, D.F., 2014. Direct physical evidence of dolomite recrystallization. Sedimentology 61:1862–1882. https://doi.org/10.1111/sed.12119.

Kelly, J.L., Fu, B., Kita, N.T., Valley, J.W., 2007. Optically continuous silcrete quartz cements of the St. Peter Sandstone: high precision oxygen isotope analysis by ion microprobe. Geochim. Cosmochim. Acta 71, 3812–3832.

Kheshgi, H., de Coninck, H., Kessels, J., 2012. Carbon dioxide capture and storage: seven years after the IPCC special report. Mitig. Adapt. Strateg. Glob. Chang. 563–567.

Kita, N.T., Ushikubo, T., Fu, B., Valley, J.W., 2009. High precision SIMS oxygen isotope analysis and the effect of sample topography. Chem. Geol. 264, 43–57.

Kupecz, J.A., Montanez, I.P., Gao, G., 1993. Recrystallization of dolomite with time. Carbonate Microfabrics. Springer, New York, NY, United States (USA), pp. 187–193.

Labotka, D.M., Panno, S.V., Locke, R.A., Freiburg, J.T., 2015. Isotopic and geochemical characterization of fossil brines of the Cambrian Mt. Simon Sandstone and Ironton–Galesville Formation from the Illinois Basin, USA. Geochim. Cosmochim. Acta 165: 342–360. https://doi.org/10.1016/j.gca.2015.06.013.

Land, L.S., 1985. The Origin of Massive Dolomite. Journal of Geological Education 33: 112–125. https://doi.org/10.5408/0022-1368-33.2.112.

Leetaru, H.E., Freiburg, J.T., 2014. Litho-facies and reservoir characterization of the Mt Simon Sandstone at the Illinois Basin – Decatur Project. Greenhouse Gases Sci. Technol. 4:580–595. https://doi.org/10.1002/ghg.1453.

Leetaru, H.E., McBride, J.H., 2009. Reservoir uncertainty, Precambrian topography, and carbon sequestration in the Mt. Simon Sandstone, Illinois Basin. Environ. Geosci. 16, 235–243.

Longstaffe, F.J., 1989. Stable isotopes as tracers in clastic diagenesis. In: Hutcheon, I.E., Nahnybida, C.G. (Eds.), Burial Diagenesis, Mineralogical Association of Canada Short Course Handbook 15. Mineralogical Association of Canada, Montreal, Quebec, Canada, pp. 201–277.

Lovell, T.R., Bowen, B.B., 2013. Fluctuations in sedimentary provenance of the Upper Cambrian Mount Simon Sandstone, Illinois Basin, United States. J. Geol. 121, 129–154.

Machel, H.G., 2004. Concepts and models of dolomitization: a critical reappraisal. In: Braithwaite, C.J., Rizzi, G., Darke, G. (Eds.), The Geometry and Petrogenesis of Dolomite Hydrocarbon Reservoirs. Geological Society, London, Special Publications 235. The Geologic Society, Bath, United Kingdom (UK), pp. 7–63.

Machel, H.G., Mountjoy, E.W., 1986. Chemistry and environments of dolomitization —a reappraisal. Earth Sci. Rev. 23:175–222. https://doi.org/10.1016/0012-8252(86)90017-6.

Mai, H., Dott, R.H., 1985. A subsurface study of the St. Peter Sandstone in southern and eastern Wisconsin. Wisconsin Geological & Natural History Survey. 47. Information Circular, pp. 1–26.

Makowitz, A., Lander, R.H., Milliken, K.L., 2006. Diagenetic modeling to assess the relative timing of quartz cementation and brittle grain processes during compaction. Am. Assoc. Pet. Geol. Bull. 90, 873–885.

Malone, M.J., Baker, P.A., Burns, S.J., 1994. Recrystallization of dolomite: evidence from the Monterey Formation (Miocene), California. Sedimentology 41:1223–1239. https://doi.org/10.1111/j.1365-3091.1994.tb01450.x.

Malone, M.J., Baker, P.A., Burns, S.J., 1996. Recrystallization of dolomite: an experimental study from 50–200 °C. Geochim. Cosmochim. Acta 60:2189–2207. https://doi.org/10.1016/0016-7037(96)00062-2.

McLimans, R.K., 1977. Geological, Fluid Inclusion, and Stable Isotope Studies of the Upper Mississippi Valley Zinc-lead District, southwest Wisconsin: A Thesis in Geochemistry. Ph.D. Thesis. Pennsylvania State University, State College, PA, United States (USA).

Melim, L.A., Swart, P.K., Eberli, G.P., 2004. Mixing-zone diagenesis in the subsurface of Florida and the Bahamas. J. Sediment. Res. 74, 904–913.

Morad, S., 2009. Carbonate cementation in sandstones: distribution patterns and geochemical evolution. In: Morad, S. (Ed.), Carbonate Cementation in Sandstones: Distribution Patterns and Geochemical Evolution. International Association of Sedimentologists, Special Publication Number 26. Blackwell Science, Oxford, United Kingdom (UK), pp. 1–26.

Oster, J.L., Kitajima, K., Valley, J.W., Rogers, B., Maher, K., 2017. An evaluation of paired $\delta^{18}O$ and $(^{234}U/^{238}U)_0$ in opal as a tool for paleoclimate reconstruction in semi-arid environments. Chem. Geol. 449:236–252. https://doi.org/10.1016/j.chemgeo.2016.12.009.

Pitman, J.K., Spötl, C., 1996. Origin and timing of carbonate cements in the St. Peter Sandstone, Illinois Basin: evidence for a genetic link to Mississippi Valley-type mineralization. In: Crossey, L.J., Loucks, R., Totten, M.W. (Eds.), SEPM Special Publication 55, Siliclastic Diagenesis and Fluid Flow: Concepts and Applications. SEPM, Tulsa, Oklahoma, United States (USA), pp. 187–203.

Pitman, J.K., Goldhaber, M.B., Spöetl, C., 1997. Regional diagenetic patterns in the St. Peter Sandstone: implications for brine migration in the Illinois Basin. In: Scott, R.W. (Ed.), Evolution of Sedimentary Basins—Illinois Basin, United States Geological Survey Bulletin 2094-A. United States Government Printing Office, Washington, DC, United States (USA), pp. A1–A17.

Pollington, A.D., Kozdon, R., Valley, J.W., 2011. Evolution of quartz cementation during burial of the Cambrian Mount Simon Sandstone, Illinois Basin: in situ microanalysis of $\delta^{18}O$. Geology 39, 1119–1122.

Pollington, A.D., Kozdon, R., Anovitz, L.M., Georg, R.B., Spicuzza, M.J., Valley, J.W., 2016. Experimental calibration of silicon and oxygen isotope fractionations between quartz and water at 250 °C by in situ microanalysis of experimental products and application to zoned low $\delta^{30}Si$ quartz overgrowths. Chem. Geol. 421:127–142. https://doi.org/10.1016/j.chemgeo.2015.11.011.

Randazzo, A.F., Cook, D.J., 1987. Characterization of dolomitic rocks from the coastal mixing zone of the Floridan aquifer, Florida, U.S.A. Sediment. Geol. 54:169–192. https://doi.org/10.1016/0037-0738(87)90021-2.

Reinhold, C., 1998. Multiple episodes of dolomitization and dolomite recrystallization during shallow burial in Upper Jurassic shelf carbonates: eastern Swabian Alb, southern Germany. Sediment. Geol. 121:71–95. https://doi.org/10.1016/S0037-0738(98)00077-3.

Reynolds, R.L., Goldhaber, M.B., Snee, L.W., 1997. Paleomagnetic and $^{40}Ar/^{39}Ar$ results from the Grant Intrusive Breccia and comparison to the Permian Downeys Bluff Sill–evidence for Permian igneous activity at Hicks Dome, Southern Illinois Basin. In: Scott, R.W. (Ed.), Evolution of Sedimentary Basins—Illinois Basin, United States Geological Survey Bulletin 2094-G. United States Government Printing Office, Washington, DC, United States (USA), pp. 1–16.

Rott, C.M., Qing, H., 2013. Early dolomitization and recrystallization in shallow marine carbonates, Mississippian Alida beds, Williston Basin (Canada): evidence from petrography and isotope geochemistry. J. Sediment. Res. 83:928–941. https://doi.org/10.2110/jsr.2013.73.

Rowan, E.L., Goldhaber, M.B., 1995. Duration of mineralization and fluid-flow history of the Upper Mississippi Valley zinc-lead district. Geology 23, 609–612.

Rowan, E.L., Goldhaber, M.B., 1996. Fluid inclusions and biomarkers in the Upper Mississippi Valley zinc-lead district; implications for the fluid-flow and thermal history of the Illinois Basin. In: Stoeser, J. (Ed.), Evolution of Sedimentary Basins—Illinois Basin, United States Geological Survey Bulletin 2094-F. United States Government Printing Office, Washington, DC, United States (USA), pp. F1–F34.

Rowan, E.L., Goldhaber, M.B., Hatch, J.R., 2002. Regional fluid flow as a factor in the thermal history of the Illinois Basin: constraints from fluid inclusions and the maturity of Pennsylvanian coals. Am. Assoc. Pet. Geol. Bull. 86, 257–277.

Shaw, T.H., 1991. Lithostratigraphy and depositional environments of the Ancell Group in Central Illinois: a Middle Ordovician carbonate-siliciclastic transition. SEPM Core Workshop no. 15. Mixed Carbonate-siliciclastic Sequences, pp. 309–353.

Shaw, T.H., 1999. Early–Middle Ordovician Lithostratigraphy, Biostratigraphy, and Depositional Environments of the Illinois Basin. Ph.D. Thesis. City University of New York, New York, NY, United States (USA).

Śliwiński, M.G., Kitajima, K., Kozdon, R., Spicuzza, M.J., Fournelle, J.H., Denny, A., Valley, J.W., 2016a. Secondary ion mass spectrometry bias on isotope ratios in dolomite-ankerite, part I: $\delta^{18}O$ matrix effects. Geostand. Geoanal. Res. 40 (2):157–172. https://doi.org/10.1111/j.1751-908X.2015.00364.x.

Śliwiński, M.G., Kitajima, K., Kozdon, R., Spicuzza, M.J., Fournelle, J.H., Denny, A., Valley, J.W., 2016b. Secondary ion mass spectrometry bias on isotope ratios in dolomite-ankerite, part II: $\delta^{13}C$ matrix effects. Geostand. Geoanal. Res. 40 (2):173–184. https://doi.org/10.1111/j.1751-908X.2015.00380.x.

Śliwiński, M.G., Kozdon, R., Kitajima, K., Denny, A., Valley, J.W., 2016c. Microanalysis of carbonate cement $\delta^{18}O$ in a CO_2-storage system seal: insights into the diagenetic history of the Eau Claire Formation (Upper Cambrian), Illinois Basin. Am. Assoc. Pet. Geol. Bull. 100 (6), 1003–1031.

Śliwiński, M.G., Kitajima, K., Kozdon, R., Spicuzza, M.J., Denny, A., Valley, J.W., 2017. In situ $\delta^{13}C$ and $\delta^{18}O$ microanalysis by SIMS: a method for characterizing the carbonate components of natural and engineered CO_2-reservoirs. Int. J. Greenhouse Gas Control 57: 116–133. https://doi.org/10.1016/j.ijggc.2016.12.013.

Stueber, A.M., Walter, L.M., 1991. Origin and chemical evolution of formation waters from Silurian-Devonian strata in the Illinois basin, USA. Geochim. Cosmochim. Acta 55, 309–325.

Stueber, A.M., Pushkar, P., Hetherington, E.A., 1987. A strontium isotopic study of formation waters from the Illinois basin, USA. Appl. Geochem. 2, 477–494.

Stueber, A.M., Walter, L.M., Huston, T.J., Pushkar, P., 1993. Formation waters from Mississippian-Pennsylvanian reservoirs, Illinois basin, USA: chemical and isotopic constraints on evolution and migration. Geochim. Cosmochim. Acta 57, 763–784.

Sverjensky, D.A., 1986. Genesis of Mississippi Valley-type lead-zinc deposits. Annu. Rev. Earth Planet. Sci. 14, 177–199.

Urey, H.C., 1948. Oxygen isotopes in nature and in the laboratory. Science 108, 489–496.

Valley, J.W., Kita, N.T., 2009. In situ oxygen isotope geochemistry by ion microprobe. 41. Mineralogical Association of Canada Short Course, pp. 19–63.

Ward, W.C., Halley, R.B., 1985. Dolomitization in a mixing zone of near-seawater composition, late Pleistocene, northeastern Yucatan Peninsula. J. Sediment. Res. 55:407–420. https://doi.org/10.1306/212F86E8-2B24-11D7-8648000102C1865D.

Warren, J., 2000. Dolomite: occurrence, evolution and economically important associations. Earth Sci. Rev. 52:1–81. https://doi.org/10.1016/S0012-8252(00)00022-2.

Worden, R.H., Burley, S.D., 2003. Sandstone diagenesis: the evolution of sand to stone. In: Burley, S.D., Worden, R.H. (Eds.), Sandstone Diagenesis: Recent and Ancient. Blackwell Publishing Ltd., Oxford, United Kingdom (UK), pp. 1–44.

Zimmerman, R.A., 1986. Fission-track dating of samples of the Illinois drill hole core. In: Peterman, Z.E., Schnabel, D.C. (Eds.), Shorter Contributions to Isotope Research, United States Geological Survey Bulletin 1622. United States Government Printing Office, Washington, DC, United States (USA), pp. 99–108.